Torsion Suspension with Activated Damper

A Major Qualifying Project submitted to the faculty of:

Worcester Polytechnic Institute

In the partial fulfillment of the requirements for the degree of Bachelor of Science

By:

Bronwen Chilton

Eli Doggart

Elliot Irving

Jakob Sperry

Wednesday, December 14th, 2022

Report submitted to:

Professor Torbjorn Bergstrom

Worcester Polytechnic Institute

Abstract

Off-road longboards require a light, compact, and capable suspension system in order to handle varied terrain with a small wheel diameter. The computer activation of the suspension through a brushless DC motor damper allows the skateboard to adapt its damping profile and even regenerate energy that is usually lost to heat. The goal of this project was to design, manufacture, and test a novel suspension on a longboard scale with active damping capable of recapturing energy. This goal was achieved through a capstan slider mechanism that translates vertical suspension travel into rotational motion at the motor and a soft bottoming-out profile without damaging the torsion bar. The team achieved this goal and developed a potential plan for future testing and design.

Acknowledgements

We would like to thank our faculty advisor, Torbjorn Bergstrom, for his continuous support, guidance, and expertise toward the fulfillment of this project. His contributions were essential to our success and learning. We would also like to thank Lawrence Sperry for graciously providing us with access to his machine shop and supplying valuable advice on a wide range of topics. Finally, we would like to thank Ezekiel Andreassen and Noah Cook for inspiring this project with their previous work, and for communicating helpful feedback throughout the duration of our MQP.

1 Introduction

1.1 Objective

The goal of this project was to design and build a prototype of a torsional suspension system with an activated inertia damper. This prototype includes a titanium torsion rod spring, a capstan drive component for rotation amplification, and a brushless DC Motor for damping control. The system was designed around the constraints for use on a traditional offroad longboard to improve suspension capabilities across a diverse range of terrain.

1.2 Rationale

Vehicle suspension systems are designed to absorb and dissipate energy inputted into the vehicle from the surface in order to create a smoother ride and improve traction. A large component of this project is damping the reaction of the suspension system, which removes energy from the system to decrease oscillation. With undamped spring systems, an impact applied on the spring will cause continuous oscillation. This causes a vehicle to bounce for a theoretically infinite amount of time after impacting an obstacle. Traditional suspension systems dissipate spring potential energy into heat using a viscous fluid damper. This project is a novel suspension system intended to provide an actively controlled damper that dissipates energy into a battery through back EMF to minimize oscillation of the system after the initial impact.

Another key component of the project is tuning the reaction force of the suspension component. We were able to design a linkage that increases the reaction force of the torsion rod exponentially throughout the suspension travel. This means that as the wheel in this scenario is forced upwards over a bump, the system provides more downward force to restore it to the rest position. At the top of the suspension travel, the torsion rod can supply near-infinite reaction force without hitting a hard end stop.

Finally, the capstan component of the system allows us to convert a small rotation of the torsion rod to many rotations of a brushless motor, which acts as an inertia damper for our suspension system. Activating the torque control of the motor allows us to precisely control the damping coefficient, as well as using regenerative braking to turn the damped, or excess, spring potential energy into electricity to be used elsewhere in the system.

The application for our suspension design is not unique to a skateboard; there are many opportunities for other applications of this system due to lightweight and precise motor and linkage control. This system is applicable for automobiles to provide active ride stabilization, off-road sport vehicles to add dynamic and personalized suspension profiles and feedback, and much more. Altering certain physical characteristics in this mechanism drastically changes its physical properties such as stiffness and damping coefficient. Although our team chose to size the design to a longboard, the methods described below have various applications across many form factors.

2 State of the Art

2.1 Suspension Linkage

2.1.1 Design Considerations

One of three main suspension components is the input linkage. In this case, the linkage connects the wheel to the torsion rod in order to transfer vertical force from the riding surface to rotational torque on the torsion rod. Ordinary longboards lack suspension due to the density of their wheels, and are limited in degrees of freedom by the minimal truck movement.

Within a suspension system for a longboard, a linkage that attaches the wheels to the spring component is necessary. This linkage should be able to transfer the vertical movement of the wheels to a force on the spring component. Many suspension systems use air shocks to handle compressive load. Due to the properties of gasses under pressure, an exponential relationship is created between the displacement of the piston chamber and the reaction force acting on the piston from the gas or fluid. As the shock suspension reaches its maximum position, it applies an exponential force to return the system to its origin. Though suspension force profiles can be tuned with valves to create a smoother ride, an abrupt increase in pressure is referred to as “bottoming out”. Figure 1 shows an ideal suspension reaction force throughout the suspension travel.

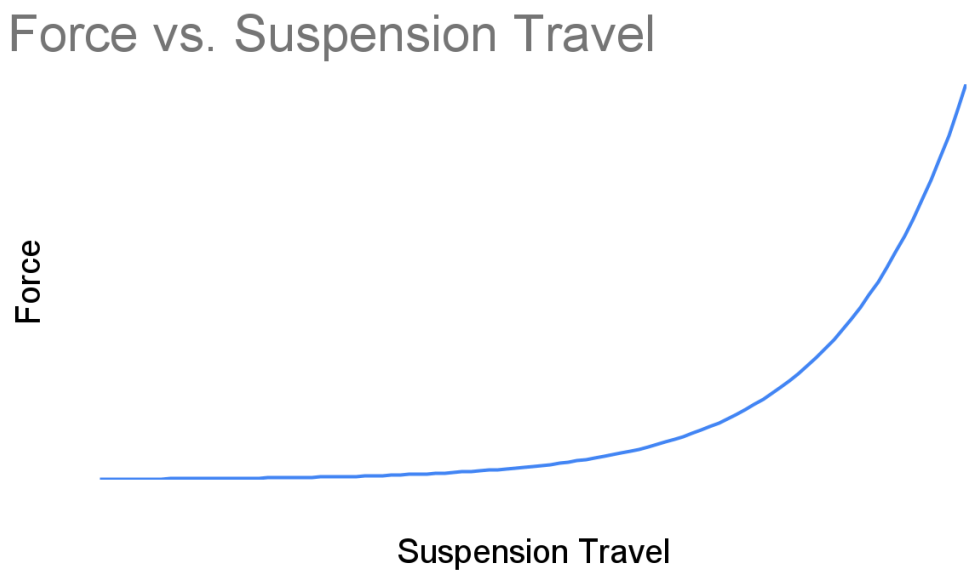

Figure 1: Graph of the Relationship Between Suspension Travel and Reaction Force

In order to achieve a suspension that bottoms out softly, it’s desirable to have the force supplied by the suspension system increase as the travel reaches the bottomed out state. Because we will be using a torsion rod (see more in 2.2.1), the working range of this spring system provides a linear relationship between applied torque to the angle of twist. In order to achieve an

exponential reaction force curve shown in Figure 1, a linkage is crucial to simulate this behavior, posing greater mechanical advantage as it moves through its range of travel.

A single lever arm could be used as the spring input, though this would provide very little mechanical advantage, especially toward the end of the travel. The length of the lever arm poses some advantage in that as its length increases, the output torque increases with a constant input force. The lever arm system does not provide the desired exponential relationship between torque and suspension travel toward the end-range of travel.

The relationship between force and torque can be quantified with the equation $\tau = r \bullet F \bullet sin\theta$, where τ is torque, r is the distance the force is applied form the point of rotation, and θ is the angle at which the force is applied. Assuming the force and angle of force application remain constant, the distance of the force applied can be changed throughout the stroke to increase torque.

With the single lever arm in mind, this an exponential relationship would be possible if the wheel somehow got closer (the link gets shorter) to the axis of torsion throughout the travel. This change would cause the force required to twist the torsion rod to increase as the wheel moves up over a bump (or down over a drop). Another way to achieve this relationship is to keep both the force and the distance from the pivot constant, and change the angle at which the force is applied. In the torque equation, the $sin\theta$ term shows that as the angle of applied force gets closer to 90 degrees, the torque applied to the system increases. So in this case, if an obstacle could somehow transmit the vertical force into one that reaches 90 degrees at maximum suspension, we could somewhat achieve this relationship. Ideally, as the suspension travels towards its maximum position, the angle of force applied trends towards 90 and the distance of applied force from the pivot decreases. A simple lever arm cannot provide the combination of both these factors, but other linkages can be explored to get closer to the desired relationship.

Straight line mechanisms such as the Scott Russell Linkage connected to the Peaucellier Linkage can achieve some of the angular advantages discussed above. The combination of these two linkages creates a system with linear motion at one end of an output link. While this linkage could be employed to isolate the vertical component of suspension travel upon rolling over an obstacle, it is highly complex, and creates various mechanical disadvantages within the links of the system. Increasing the number of moving components increases the likelihood of part failure and makes linkage maintenance more difficult. Environmental hazards including dirt, dust, and debris are likely to come in contact with the suspension system throughout regular use, so avoiding complex systems that are easily susceptible to damage is important.

In order to create a linkage that allows for exponential reaction force from a torsion bar linkage by changing the *r* variable in the torque equation, a variable length link is necessary. Common variable length links include pistons, lead screws, and slider mechanisms. Pistons are often integrated into the linkages of steering mechanisms, and consist of two or more concentric cylindrical components that slide in and out of one another, allowing for telescopic motion.

A lead screw is a mechanism often used to convert rotational motion into linear motion and consists of a nut and a screw shaft. When the screw shaft rotates, the nut moves translationally along the screw axis. Although simple, this variable length link loses energy to friction through the interaction between threads on the nut and screw, making them more applicable to low power applications. Some friction forces may be overcome by using a hydrostatic lead screw, where fluid is continuously supplied to the mechanism to decrease friction. However, due to the complexity of this mechanism, there are more viable solutions than the lead screw for our application. (Liu, Y., Feng, X., Li, Y. *et al.)*

Slider mechanisms usually consist of two components, the slider and the constraining rail or slot. In the case of a pin slot slider, the pin can rotate freely, though translational movement is constrained linearly by the profile of the slot. Many slots are straight lines, but more complex, curved paths may be used in some applications.

In slotted slider linkages, the length of the link changes as the pin link rotates. As the link gets shorter, the distance where external force is applied gets closer to the pivot. Thus, the force required to enact the same amount of torque about the pivot point increases. If the torsion rod is the pivot point, as the stroke of the wheel reaches its maximum — and variable length slider linkage shrinks — the force required to twist the rod increases exponentially and the suspension stiffens. This achieves the desired relationship between force and suspension travel.

The disadvantages of slider mechanisms include friction between the pin and slot and material weakness in small components. If not properly constrained, a pin slot slider is susceptible to movement in other directions that may cause binding, stress concentrations, and unexpected movement. Thus, fixtures are necessary to avoid premature failure in this style of component.

When designing a linkage for this application, the form factor of a skateboard must be considered. This includes expected vertical travel and clearance between the linkage and the board/ground. Traditional skateboards consist of simple, small components used to attach the wheel to the board. To create a suspension system that allows for similar performance to traditional skateboards, the linkage must fit these general constraints.

2.1.2 Existing Suspension Linkages

Many other forms of suspension/ suspension linkages have been created to solve problems similar to the ones we are trying to solve. Mountain bike suspension consists of two shocks attached to a wheel on either side. Because the connection between the suspension and the wheel orients the pistons to a nearly vertical orientation, the suspension can directly transfer the linear vertical force on the wheel into the pistons.

Traditional skateboards and longboards have trucks connecting the wheels to the board. The only suspension in this system is within the rubber of the wheels, but the same need for connection applies. Off road skateboard suspension does exist and usually consists of a piston/spring design with connections between the suspension and the board.

An example of a popular design for suspension on an off road skateboard can be seen in the popular Bajaboard. (*Bajaboard*, G4 Range) Large tires are used for off-road conditions over traditional small, dense, rubber or polyurethane wheels of traditional longboards. These large, softer pneumatic tires also provide damping to low amplitude, high frequency vibration, such as light gravel road texture. The additional suspension system is used to damp larger bumps like rocks or potholes.

In this example, the connection of the suspension and the board consists of two links. The upper link pins the top of the shock to the board. The lower link pins the bottom of the shock to the wheel mount allowing for vertical compression of the shock. This suspension was originally based on off-road buggies, where linear vertical motion is transferred into a shock using a similar linkage arrangement.

Formula 1 (F1) racing cars are known to use and develop torsion rod springs for their suspension. This competitive and well-funded niche industry is known for its rapid mechanical design innovations and was of keen interest for our application. Figure 2 shows a simplified diagram of a F1 suspension and steering system highlighting a ternary link that transmits vertical wheel force to torsion through a pushrod.(Perkins, Chris.)

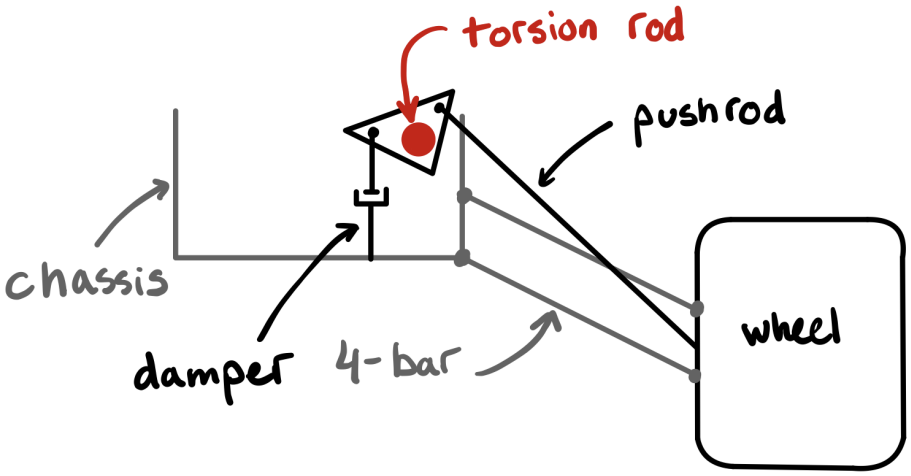

Figure 2: Simplified F1 Torsion Suspension System

There are many similarities between suspension-to-chassis connections methods listed above. Each of these linkages transfer the linear motion of the wheel into a spring component. The F1 suspension linkage is most applicable because of its transfer of linear vertical movement to rotational movement of the torsion rod.

2.2 Torsion Rod Spring

2.2.1 Design Considerations

The spring in a suspension system is used to store energy from the riding surface to improve the stability and comfort of the ride, and helps maintain wheel traction to the riding

surface. As a vehicle's wheel goes over a bump with no spring, the entire vehicle chassis would rigidly move up over the bump and be displaced the height of the bump. Including a spring in the system allows the vehicle to generally maintain its vertical position, as the energy that would be used to displace the chassis is stored as spring potential energy.

As the wheel moves up over an obstacle, the spring stores energy and compresses. However, after compression, the energy is released, re-extending the spring past its original resting position. This reaction spring force can often push the wheel back down into the riding surface to maintain traction, but can cause oscillation for the main vehicle chassis.

When considering springs in a suspension system, one must take into account the continuous oscillation after compression without damping. Excessive oscillations in an undamped system can result in an undesirable experience for passengers. Additionally, oscillations vary the normal force of the vehicle back on the terrain, which increases the likelihood of traction loss, and therefore control of the system. See Figures 3 and 4 for diagrams of a damped and undamped spring.

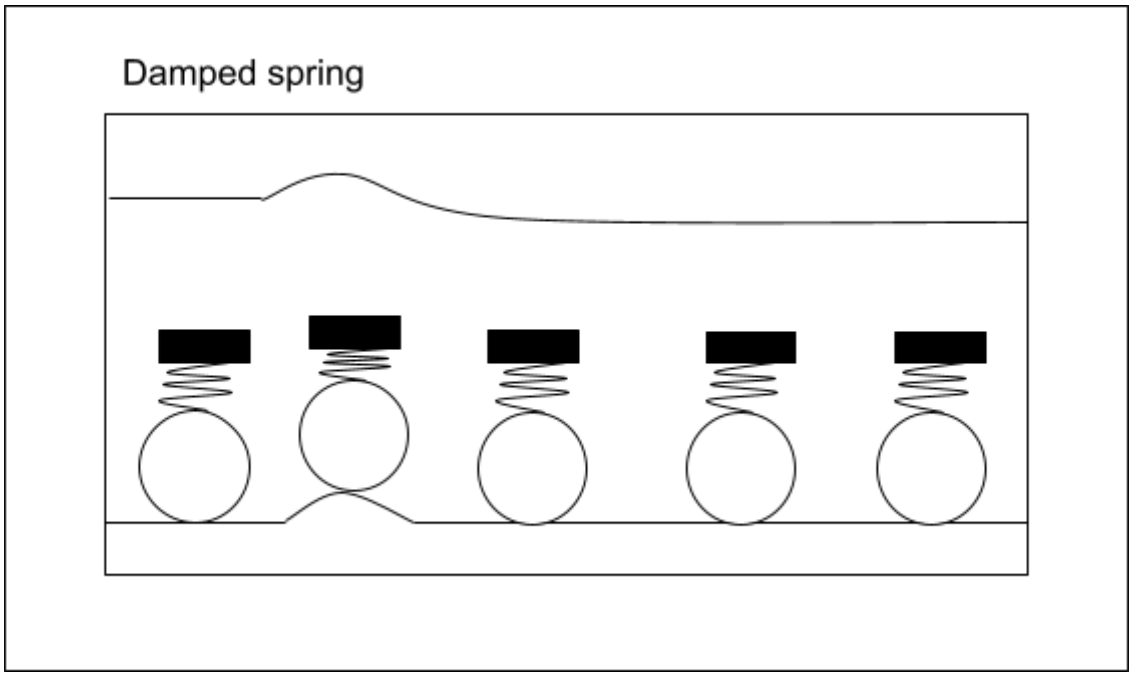

Figure 3: Motion Path of a Damped Spring

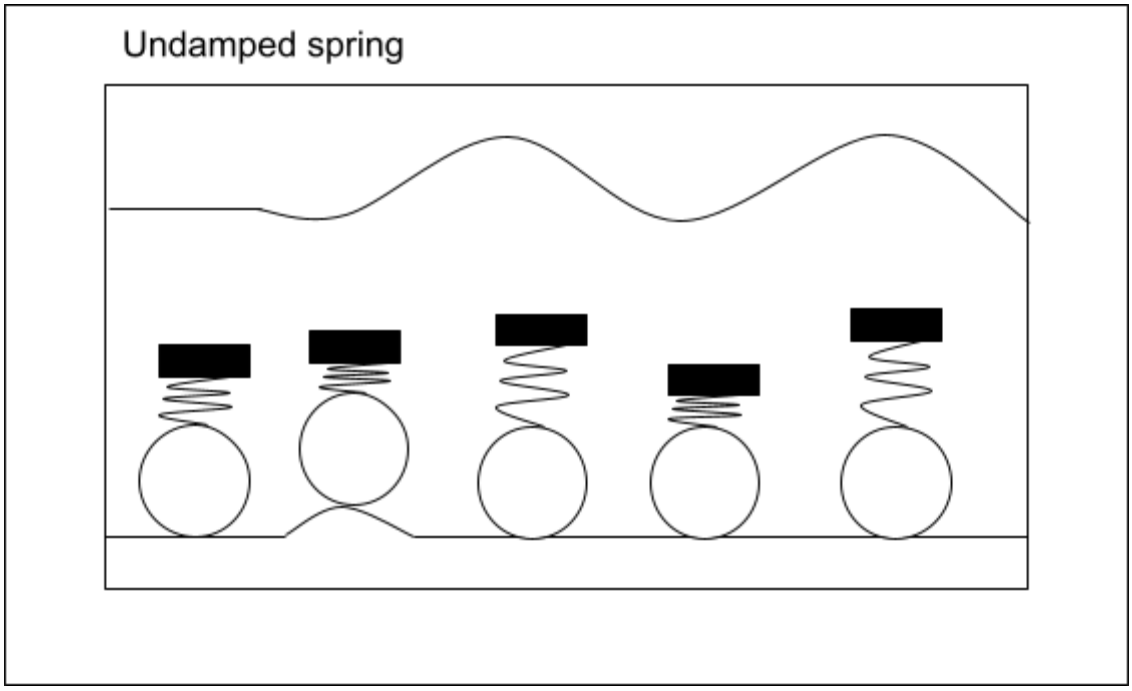

Figure 4: Motion Path of an Undamped Spring

Infinite oscillation, if not damped, can also be observed in a torsion rod spring. Although the characteristics and movement of the torsional spring differ from linear springs, similar concepts can be applied. A torsion rod spring uses the torsion of a rod as the spring force in the system. Instead of creating a linear reaction force, the torsion rod applies a reaction torque under twist. The following equation describes the properties of a torsion rod spring,

$$\frac{T}{J} = \frac{\tau}{r} = \frac{G \times \theta}{L}$$

where T is torque, J is the polar second moment of area, τ is the shear stress, r is the radius of the rod, G is the shear modulus, θ is the angle of twist in radians, and L is the length of the rod.

The variable J describes the polar second moment of inertia, which is the torsion rod's resistance to torsion. It is affected by the cross sectional shape and area of the rod, and can be related to its rotational stiffness. The shear stress on the rod, τ, is related to the shear modulus and is a function of the amount of twist. As the rod twists to a greater angle from its original position, the amount of shear stress along the radius of the rod increases. The greatest shear stress is experienced on the surface of the rod.

The length of the rod, L, also has a large impact on its performance. Based on the equation, the longer the torsion rod, the greater angle of twist required to cause the same amount of torque and shear stress on the rod. Both of these parameters are also related to the rod radius. The relationship between torsion bar radius versus length and shear stress to achieve a desired torque and angle of twist can be seen in Figure 10 in Section 2.5. All of the properties in the equation listed above must be taken into consideration when designing a torsion rod for use in a suspension system.

2.2.2 Torsion Rod Material Selection

In order to be effective as a spring, the torsion rod must have a mid-range Young's Modulus to allow for an acceptable amount of rotation. The dimensions of the rod can be changed to alter its spring-like characteristics, but the material itself needs to have enough elasticity to act as a spring without deformation. Titanium fulfills these requirements, and because of availability of materials from the previous independent study project (Section 2.5), we chose to use an 8mm titanium torsion rod.

2.2.3 Torsion Rod Fastening Mechanism

In order to act as a spring, the torsion bar must be fixed at one end, while the suspension linkage input twists the other. One simple method to fix the end of a cylindrical rod is a clamp. Although this method is useful in many cases, high torsion can cause the rod to slip within the clamp. Precise tolerancing and knurling can be employed to increase surface friction and therefore the torque capacity of a clamped interface. Knurling is a forming operation done to deliberately mar the surface of the rod in a repeated pattern. Knurling slightly increases the rod's diameter and surface area, two factors that lead to an increased frictional force.

Additional elements such as keys, pins, and set screws can be used to further prevent slipping. Keys opposes torsional forces once inserted into the keyseat and decreases the likelihood of slip unless deformation of the key, keyway, or keyseat occurs. Set screws into a planed surface on the rod can also be used to increase the force between the rod and the clamp/hole and therefore increase friction. See Sections 2.5, 3.3, and 4.3 for explanations as to why a clamping mechanism was chosen and tested.

2.3 Capstan Rotation Amplifier

2.3.1 Design Considerations

Rotational velocity can be amplified in many ways, each way with benefits and negatives. Traditional gearboxes have advantages such as continuous rotation, strength, and manufacturability. However, spur gears have a significant amount of friction in between the teeth of meshing gears. As the driving gear spins, the surface of the teeth apply a force on the other gears. Friction between the teeth is caused by the surfaces of the teeth sliding against one another as they continue their motion path. (Kahraman, A., Li, S.)

Backlash also plays a role in energy loss in traditional gear boxes. Figure 5 shows two spur gears meshing properly. Accurately aligned gears have a larger space in between teeth than the width of the teeth themselves. This larger gap allows the gears to rotate freely and helps prevent binding. Although necessary for the function of the gears, this gap allows for some initial rotation of the driving gear before coming in contact with the driven gear. This phenomenon is referred to as backlash and makes the entire system less reactive to direction changes and can lead to significant energy loss from these events.

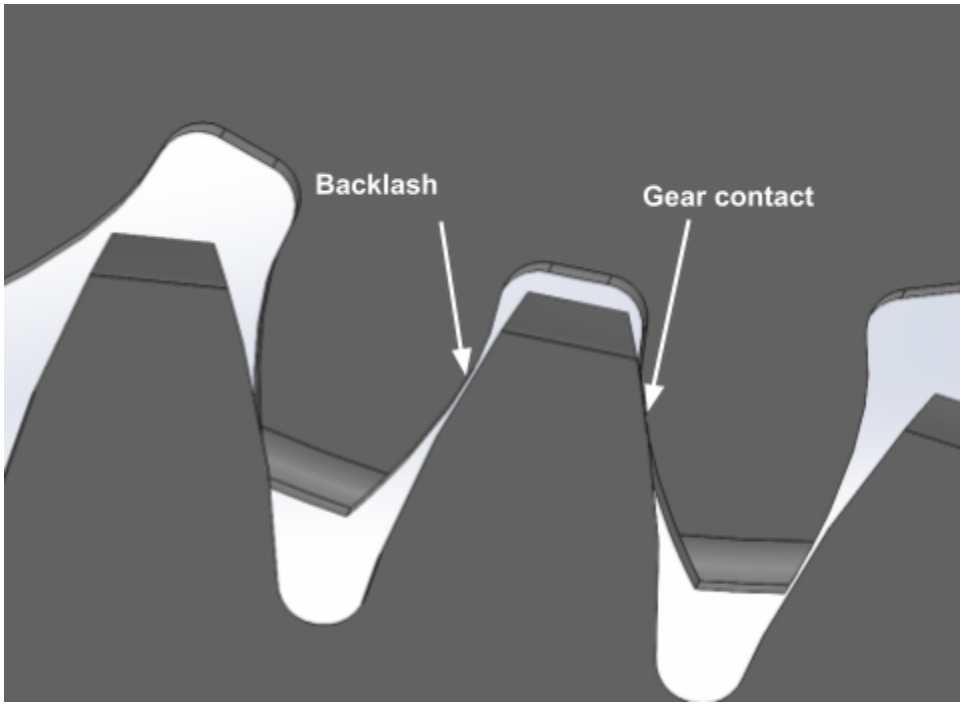

Figure 5: Backlash in Spur Gears

Another limiting factor of traditional gearboxes is their gear ratio, which is defined as the input rotation over the output rotation. The diametral pitch of the gears limits this ratio in a single stage. (Simmons, Colin H., et al.)

Capstan drives can be used as an alternative solution for amplifying the rotational velocity, while minimizing friction at the input-output interface and eliminating sliding interfaces. Capstan drive ratios can be much larger as the two bodies interface as two rolling cylindrical surfaces and are not limited by diametral pitch. The fundamental concept behind this drive is the Capstan Equation (equation 1), which is used to determine the hold-force to load-force parameters of a flexible cord wrapped around a smooth cylindrical surface.

Equation 1:

$$F_{load} = F_{hold} * e^{\mu * \phi}$$

F_{Load} : The amount of load the system can handle before slipping

F_{hold}: The holding force on the opposing side of the capstan

μ: The coefficient of friction between the drum and the cable

ϕ: The total angle of wrap in radians

A capstan drive consists of two drums connected by a cable. The cable originates from one side of the large drum and follows the outer arced surface to then meet the smaller drum. The cable then wraps around the small cylindrical drum, following the grooves that wrap helically around its surface. The cable is usually wrapped at least twice around the small drum to ensure

sufficient friction force between the drum and cable to reduce slip, though more loops can be used to create a greater hoop stress and therefore a resistance to sliding along the drum's surface.

Once tensioned properly, the cord's resistance to slipping creates a zero-backlash rolling interface between the drums. After wrapping around the small drum the cable follows the surface of the large drum once again and terminates on the opposing side of the large drum. Each drum is mounted to rotate about their center points, so when the input drum initiates rotation, the output drum "rolls" along the surface, driven by the cable. This rolling motion limits loss of energy due to friction between the surface of the two drums.

The relationship between the amount of wraps around the cylindrical drum and the friction force between the cable and the drum is exponential. Depending on the material chosen for the surface finish of the grooved drum and the fiber chosen for the cable, the coefficient of friction will also change. Increasing the amount of wraps around the drum increases the hoop stress around the small drum, and thus, increases the static friction force. This static friction prevents the cable from slipping around the drum and ensures consistent and smooth rolling interface between the drums. (L. Hunter)

The method of driving the output with a cable also ensures there is no backlash.

When amplifying rotational velocity, the input drum is the larger of the two. For this application, the smaller of the two drums must be a full cylinder while the larger can be a section of a cylinder. The angular section dimension of the large drum limits the range of rotation of both components. Once the small drum has reached the terminating point of the angular section of the large drum, rotation cannot continue in this direction. For the purpose of an oscillating rotation, only a certain range of rotation is required before reversal occurs. The nature of the capstan allows for reversal in the direction of the rotational input in addition to the ability to back drive the mechanism.

Backdrivability can be defined by the ability of a mechanism to work in the reverse direction. In this case reversing direction refers to the direction of force traveling through the system. This means the output drum can also apply force to the input drum. For this application, the input drum will be attached to a linkage, inputting rotation from variable forces from the road on the wheel. This rotation will be transferred and amplified to the output drum which spins the motor damper component of the assembly. As damping occurs, the motor will apply a resistive force back onto the large drum, therefore reversing the direction of force travel, hence the need for zero-backlash backdrivability.(T. Ishida and A. Takanishi,)

2.3.2 Negating Motor Shaft Moment with Dual Capstan Drive

Capstan drives with a single cord suffer from the cord tension creating a moment on the motor drive shaft, as demonstrated in Figure 6a, which translates to a radial load on the motor shaft bearings. While small, eliminating this will increase the longevity of the bearings and decrease the undesirable load on the shaft. To eliminate the moment on the motor shaft, an opposing cord configuration can be applied, as shown in Figure 6b. We refer to this configuration as a dual capstan drive, and this model assumes that the distribution of cord tension is equalized

as F_T throughout the system. All axial loads on the bearing created by the tension force acting at an angle are negated.

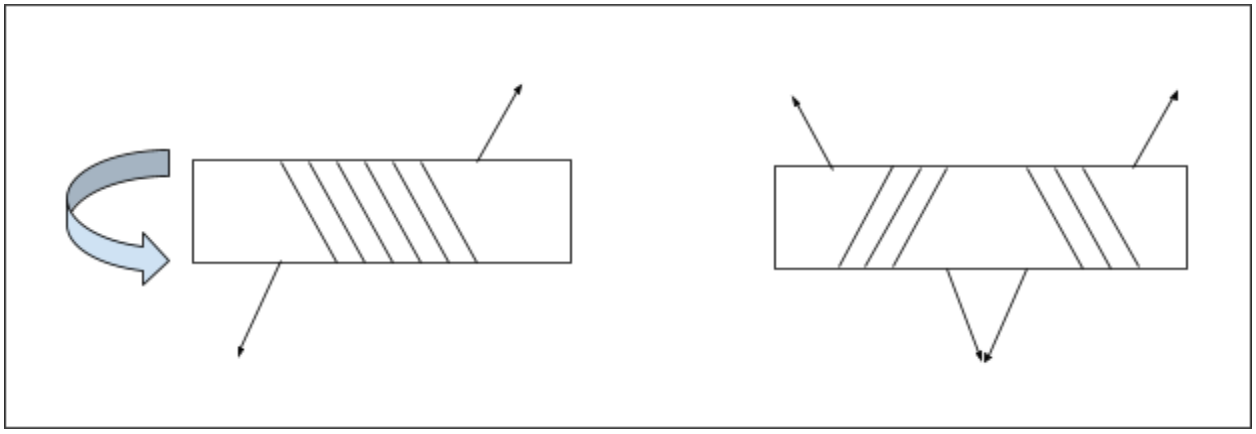

Figure 6a (left): Single Wrap Capstan Concept
Figure 6b (right): Double Wrapping Capstan Concept

The dual capstan drive has the added benefit of distributing the tensile load across two cords rather than one, halving the required strength for each cord and therefore their diameter. Flexible cords also have a recommended minimum ratio of curvature to rope diameter that can, if ignored, can lead to diminished tensile strength and lifespan (A. Mazumdar et al.,). Utilizing smaller diameter cords for lower strength requirements also means they are less susceptible to wear around the sharp bends wrapping around the small drum component and contribute to a more compact design footprint.

2.3.3 Fiber Selection

Depending on the intended use of a capstan, different cord material, braid type and diameters are recommended. For slow rotation with a large load, a larger diameter cord is recommended. For applications with fast, precise, and relatively low load requirements, a smaller diameter cord is recommended (N.Denerley).

Many metallic cables have high tensile strength but are limited in their flexibility. Accelerated wear can occur due to excessive bending of metallic cables, which is why synthetic fibers can be considered a viable option for this application.

Braid pattern does have some effect on the tensile properties of the cord, though negligible for our application. The cord is required to withstand the driven torque of the motor on the capstan to damp the system oscillations. The capstan drive can also be driven by two cords, eliminating the internal moment on the motor shaft as described in section 2.3.2 and halving the required minimum cord tensile strength. The minimum tensile capacity of the cord depends on the maximum torque applied by the motor at an effective distance of the small drum radius, which can be seen in equation 2.

Equation 2:

$$Max.\ tensile\ load\ through\ each\ cord\ = \frac{maximum\ motor\ torque}{effective\ radius\ of\ small\ drum} * \frac{1}{2}\ [for\ 2\ cords]$$

$$= \frac{5\ [Nm]}{0.005\ [m]} * \frac{1}{2}$$

$$= 500\ [N]$$

Cord thickness should be determined based on the required tensile load of each cord. Due to numerous variables, such as weave pattern and synthetic material grade, there are few resources and equations that govern Dyneema® tensile properties. The team purchased 1mm diameter Dyneema® whipping twine rated for 160 kg, which is equal to handling ~1,570N of tensile load. Therefore the safety factor for the capstan drive cord is around 3.

2.3.4 Capstan Material and Surface Finish Selection

Aluminum is an inexpensive, easily accessible, low density, easy to machine metal that well exceeds our material needs for strength. This makes it ideal for the capstan which needs to be lightweight, requires significant machining, and needs to withstand many use cycles.

The end of the capstan will be one of the fastest moving parts of the suspension with the possibility of gathering a lot of momentum. In this system momentum resists oscillation which is undesirable in a suspension. Therefore it is preferable to decrease the mass of the fast moving components like the capstan by making them out of low density materials like aluminum.

A large part of the engineering design process is iteration and testing. Because we predict we will redesign and test the capstan component multiple times, and resource availability is a factor in our decision, we need to choose a material that is easy to acquire and work with. The capstan will require a significant amount of machining, so faster machining will lead to more time for iteration. Aluminum fits this criteria perfectly being inexpensive, easy to access, and easy to machine.

Another possibility is to 3D print the large and/or small drum either out of metal or plastic. Because of the nature of additive manufacturing, complexities within the capstan design (ie. helical grooves wrapping around the small drum) can easily be produced. This advantage differs from the aluminum machining process which is typically a subtractive manufacturing process, requiring very specific and sometimes difficult to produce tool paths. One concern of printing the parts rather than machining them from stock is the presence of extreme hoop and shear stresses, specifically on the small drum, because of the way the cord will be tensioned and fully wrapped around the body of the part. One way to mitigate this obstacle is to print the components using metal, rather than plastic.

Although the small drum can be manufactured solely using the 3D printing operation, complications may arise with the large drum component because of the multiple operations it will perform throughout a use cycle. The large drum consists of the outer surface and tensioning system, a slot for the input link to interact with the capstan, as well as a clamp component for the torsion rod. See Figure 20 in section 3.2.

3D printing is useful for the outer surface of the large drum in the capstan because it does not take significant load, and is mainly used as a guide for the cord in the capstan. The slot, however, will be taking significant load from the input link and needs to have a consistent, smooth surface finish to allow for a proper sliding motion of the pin within the slot. The clamp component will also take a significant amount of load in order to secure the torsion rod. This

component also requires a very precise interface, because the tolerance needed to prevent slip in the torsion rod is very small. For these components, machining the large drum out of aluminum stock is more advantageous.

A combination of the two manufacturing processes can be used for the production of this part by splitting the large drum into two separate parts. The “crust” can be 3D printed while the large drum body can be machined. By splitting up this component, we can produce a part strong enough to withstand the required loads, while also cutting some weight from the system to decrease angular momentum.

2.3.5 Anchoring and Tensioning Mechanisms

The function of the capstan component depends on the tensioning of the cord wrapping around both the large and small drums. Inorder to maintain tension, capstans require anchoring and tensioning mechanisms. In many capstan designs, the use of epoxy injected fibers in an anchoring slot is present. By separating strands at the end of the cord after passing through a sort of collar, epoxy can be applied to maintain a wider diameter on the end of the cord. This increase in diameter prevents the cord from slipping through the collar and releasing tension in the system. Figure 7 shows this process.

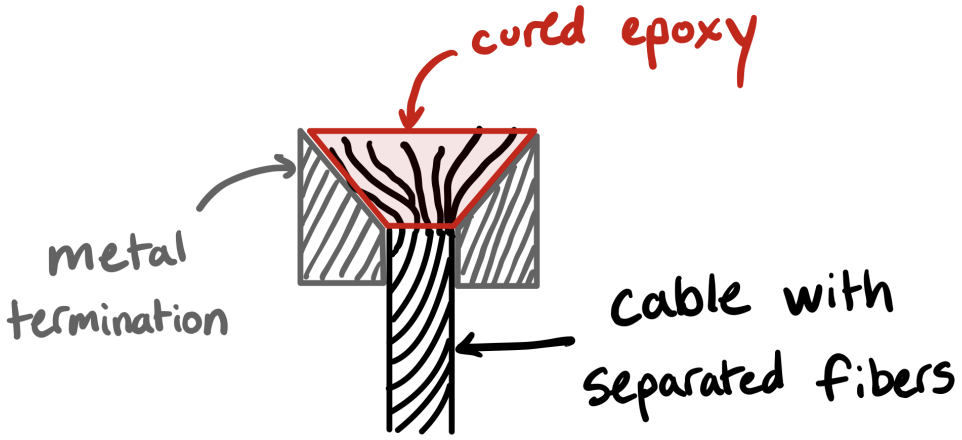

Figure 7: Epoxy Embedded Cable Anchoring System

Many tensioning systems incorporate this epoxy embedded anchoring system. After the end of the cord is terminated, the cord can be wrapped around a rolling cylindrical drum and tightened to the desired tension. Figure 8 shows the cylindrical component attached to a rail system. To increase the tension in this system, the user can unscrew the retaining bolt and move the cylinder to the desired tension. This system is advantageous because it allows for adjustability in tension and decreases the force applied to the anchor because of the additional frictional force applied to the cord by the tensioning cylinder.

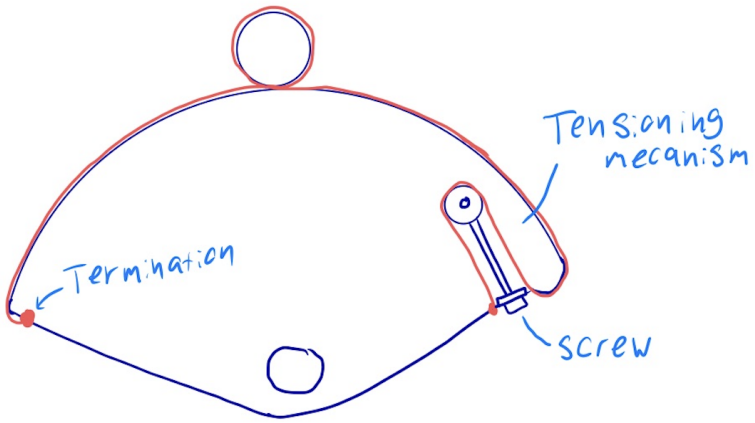

Figure 8: Railed Cylindrical Capstan Tesnioning System

Automatic tensioning systems are also widely used for this application. Shown in Figure 9, one end of the cord is attached to a spring. The spring applies a constant tensioning force on the cord throughout the use cycle. This method is advantageous because the spring can still apply a tensioning force to the cord even after it settles and stretches.

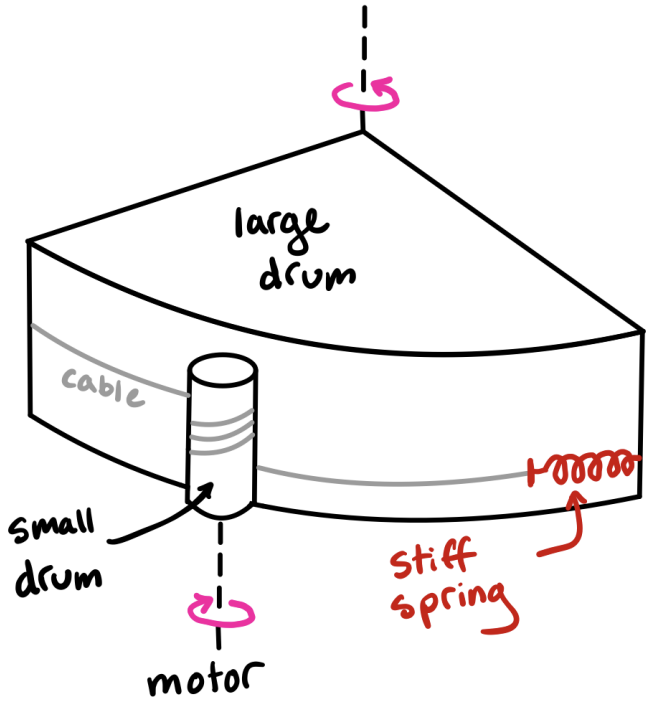

Figure 9: Spring Loaded Automatic Tensioning System

Another method of tensioning/anchoring, traditionally used in musical applications, is a tuning peg. Wrapping the cord around its end applies a constant frictional force to the end of the cord and sufficiently anchors itself. After reviewing tuning pegs and other similar mechanisms, it is clear that this anchoring mechanism is more than capable for use in a capstan. In many cases,

the cord is more likely to break before slipping from the anchor point. The tuning peg also acts as a tensioner, and has the ability to twist the shaft holding the cord to increase tension.

In any case where the cord will be wrapped around the edges of the large drum, or in this case the edges of the crust, a chamfer is important to limit wear on the cord. By limiting the introduction of any sharp corners, the cord will be less likely to attain damage from the capstan surface and prevent premature failure.

2.4 Brushless Motor

2.4.1 Design Considerations

Brushless motors consist of a stator with electromagnetic coils and a rotor with many fixed permanent magnets. Three-phase AC current is used to control the motor which means that these motors require a special motor controller. A brushless motor controller is used to send current to the correct coils to advance the rotor. There are two types of brushless motor controllers commonly used, back-EMF feedback, and field-oriented control (FOC) feedback. Back EMF controllers do not use an encoder and rely on the back EMF through the coils to measure the position of the rotor in order to correctly send current to the stator.

FOC controllers use an encoder to measure the position and are better at applying low-speed torque. FOC controllers are much more advanced than back EMF controllers, but they are much more expensive. Applications in which the motor will spin at high speeds and the velocity is the controlled perimeter, back EMF controllers are a good choice due to their lower cost. In applications where a motor will be used at lower speeds or to do complex motion, a FOC controller is suited.

Brushless motors are a good choice for small, fast-moving, and high torque robotic applications due to brushless motors' high power density and ability to be precisely controlled with a FOC controller. Brushless motors are also very good at power regeneration and are commonly used for motor braking in electric vehicles.

2.4.2 Brushless Motor Dynamic control

FOC controllers are powerful ways to control brushless motors because of their precise positional feedback. FOC controllers use encoders attached to the motor to measure the position of the rotor relative to the stator. This allows FOC controllers to provide high torque at all speeds, including stationary. ESC controllers rely on the back EMF feedback of the permanent magnets which means that they are imprecise at lower speeds.

FOC controllers also allow for multiple control methods such as torque control, velocity control, and position control. These control systems will allow us to activate the suspension and control the damping coefficient in multiple ways. It will also allow us to back drive the system to do preventative or reactive suspension tuning.

High end bicycle trainers are a good example and inspiration for this technology. We looked at the Tax Neo 2 smart trainer for inspiration on using permanent magnet brushless technology to do torque control damping instead of motor driving. This trainer uses what is

essentially a brushless motor to apply resistance to a bike wheel to simulate the road. The resistance is controllable to simulate the feeling of hills while biking. The trainer is also capable of driving the wheel to simulate the feeling of a downhill. The technology we are using is very similar to how the Tax Neo 2 implements brushless motor dynamic control. We will be using adaptive resistance to control the damping coefficient. This also leaves the possibility open to control the suspension with the motor in order to drive the position of the wheel based on inputs from the road.

2.4.3 Regenerative Suspension Using Brushless Motor

Brushless motors are also capable of acting as generators. If a brushless motor is being driven externally, the controller can apply a resistance and convert the rotary energy into electrical energy. This both slows the motor by applying a resistance to the rotation and generates electricity. If the motor controller is connected to a battery, the collected energy will be put into the battery for storage. This allows us to convert small vibrations from the road battery power while damping the vibrations.

2.5 Electric Off-Road Skateboard Independent Study Project

The inception of this MQP project originated from an Independent Study Project (ISP) completed by Ezekiel (Zeke) Andreassen, Elliot Irving, and Noah Cook during C-term 2022 at WPI. This project aimed to design the components necessary for an electric off-road skateboard capable of handling hard-pack or grassy terrain at speeds upwards of 30mph.

Zeke had been brainstorming a torsion rod suspension system inspired by Formula 1 racing as a skateboard suspension for some time. The team soon became interested in pursuing an inertia damper, or inerter, over an oil shock absorber for the suspension system. This technology was known in the Formula 1 racing industry as the “J-Damper” and was developed by Cambridge University and McLaren in 2005. However, this technology was banned in F1 racing shortly after its implementation. The supposed rationale for the ban ranges significantly, from safety concerns regarding large spinning masses in the front of the racecar to general cost-cutting regulations (Collins),(Kay).

The idea of adapting this system further into an actively-damped suspension system soon followed.

The premise of an inertia damper is that suspension compression spins up the mass in one direction, and applies an opposing torque upon relaxation, overcoming the initial angular momentum and reversing the angular velocity. This results in a strong attenuation of suspension oscillations in the system, regardless of the size of the input. Various algorithms for an inertia damper were considered for our inertia damper design, including the effects of a single direction damping or clutch mechanism. This would involve an undamped compression phase and a damped release phase. This could allow for full utilization of the suspension characteristics during compression, without the resistance to spin up that a damper provides, yet still allow for

damping during the rebound phase. We also considered tuning the damping coefficient using flywheels or varying mass.

In order to amplify the small angle of twist of the torsion bar suspension into multiple rotations of a flywheel, the system requires a gear train. We originally designed a multi-stage spur gear train to amplify the rotation of the torsion bar throughout its travel. However, as outlined in 2.3.1, spur gears are limited in the shear strength of the teeth and are susceptible to inherent backlash at each stage. These limitations are most apparent at the first stage of the gear train, where the torsion bar is applying the greatest amount of torque to the gearbox. Therefore, the first gear tooth had to be oversized to transmit the needed torque without shearing. Consequently, the capstan drive used in our MQP was considered to eliminate spur gear tooth failure.

We selected a four-bar linkage that required 30 degrees of torsion bar angle of twist. Zeke created a host of MATLAB scripts for linkage kinematics and torque values through each link member vertical travel. We found that the maximum torsion bar torque must apply 81.75kgf to support a quarter of the rider's weight. In order to select an appropriate length and diameter of torsion bar for the desired applications, we created a MATLAB script to visualize the length of the effective torsion bar and shear stress associated with these parameters for a range of torsion bar diameters. Figure 10 visualizes these parameters and allows us to select a torsion bar that was short enough to fit our application and verify that the shear stress fell well within the elastic properties of the titanium shaft.

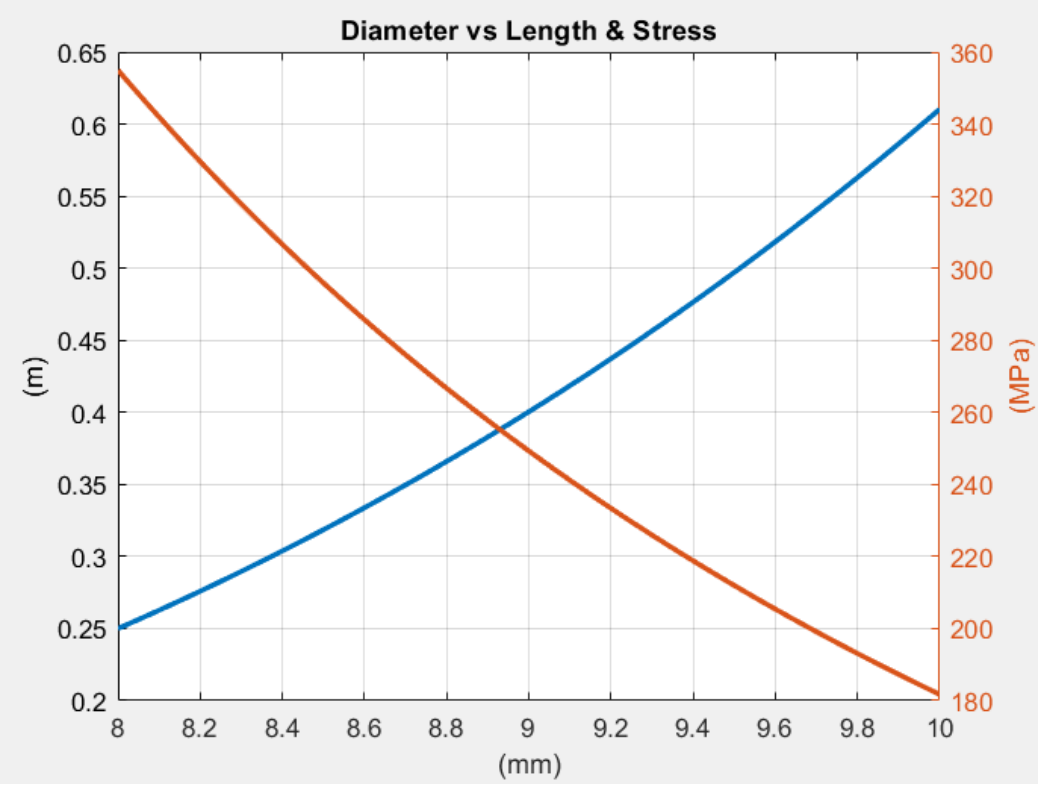

Figure 10: Visualizing the Effect of Torsion Bar Diameter on the Required Effective Length and Corresponding Shear Stress at 30 Degrees of Twist.

The team brainstormed various methods of securing the fixed end to the skateboard, including a stir welded bracket, titanium welding to the frame, cutting a spline into the fixed end of the shaft, and clamped collar. The team decided to pursue a clamp collar on their test rig after calculating the required clamping bolt torque required to resist the full reaction torque of the torsion bar. To understand the effectiveness of the clamping mechanism, they placed permanent ink markings on the mated surface to act as a visual marker for any sizable slippage throughout the full range of the system. The initial test revealed slipping between the torsion bar and the clamp. Reassembling the test fixture with cleaned frictional clamping surfaces with denatured alcohol showed no slipping. The team concluded that with clean surfaces, the clamping mechanism performed as expected and would be a valid securing mechanism for the needs of this MQP.

The work done in this Independent Study Project revealed critical design areas requiring further development, including an improved linkage design for ideal suspension force characteristics, a gear train design minimizing bulk material and backlash, and a greater need to understand fundamental damping methods.

3 Methods

3.1 Suspension Linkage

3.1.1 Perpendicular Linkage Design

3.1.1.1 Linkage Theory

We created a linkage with a perpendicular link couple driving the rotation of the torsion bar. After drawing this configuration on a linkage software it was clear that as the stroke of the “wheel” (or link that would theoretically be connected to the wheel component in the scope of a suspension system– this link would be taking vertical impact due to a bump or drop on the riding surface) continues, the change in angle of the link attached to the torsion rod increases. This increase in change of angle is important because it signifies that more reaction from the torsion rod will be input into the system as the wheel reaches its maximum or “bottomed out” position.

3.1.1.2 CAD Modeling and Additive Manufacturing

Using CAD, we modeled the concept explained above and created an assembly with the design intent for additive manufacturing and later testing. Each component was created as a part file and added to an assembly with mates ensuring the assembly could move in the desired path without interference between parts. This model was designed around 8mm shaft diameter ball bearings and includes hook features to attach rubber bands for testing.

We then printed a 3D model of this perpendicular linkage design for testing purposes using a Prusa i3 with PLA. After printing, bearings were pressed into the print and hot glue was used as needed to ensure security between the print and the bearings. A rubber band was

connected, as shown in Figure 11, to mimic the spring force that would be imposed by the torsion rod in the theoretical situation.

Figure 11: 3D Print of Perpendicular Linkage Concept

3.1.1.3 Testing

A visual confirmation of the increased angle relationship was performed by setting up a ruler next to the linkage on a flat surface, without the rubber band attached. In this test, we moved the linkage attached to the wheel vertically, starting from the maxed out bottom position and this position was measured. To compare the bottom of the stroke to the top of the stroke, we performed two movements of ½". For the purpose of this test, we compared the change in angle of the link that would be connected to the torsion rod in each of the two cases.

3.1.2 Curved Slider Linkage Design

3.1.2.1 Linkage Theory

The curved slot slider was designed to acquire an exponential relationship between reaction force and displacement. By changing the path of the slider, you change the angle of force applied to the slot link and therefore the torque applied to the torsion rod. When brainstorming the curved slot, drawings were made in conjunction with free body diagrams to conceptualize the direction of forces within the system.

3.1.2.2 CAD Modeling

We modeled this prototype using SOLIDWORKS, and designed it to use the same bearings and rubber band testing strategy as stated in section 3.1.1. This model was toleranced and designed to be 3D printed and clamped in a vice for testing.

3.1.3 Slider Linkage

3.1.3.1 Linkage Theory

While deciding on a suitable linkage, the idea of a variable length link came up that would allow for variable mechanical advantage over the travel of the suspension. A decreasing mechanical advantage from the wheel to the torsion rod would lead to a natural soft bottom out of the suspension. The initial idea for this slider was modeled in a linkage software with promising results. The desired result of an increase in link length (leading to an increased torque when force is the same but distance from pivot point is larger) was acquired and demonstrated using the linkage software.

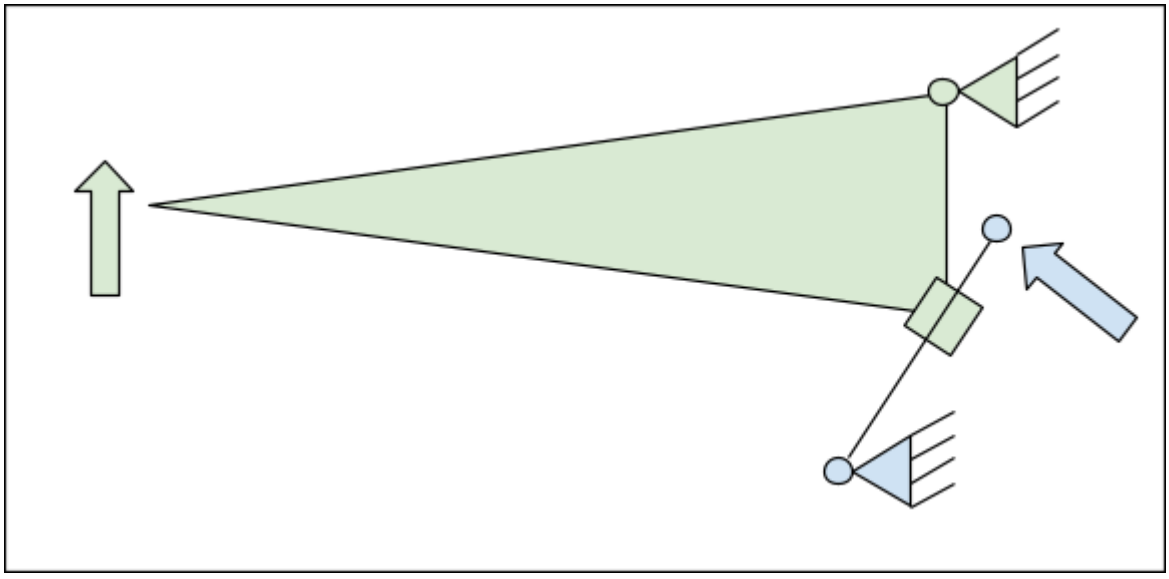

Figure 12: Linkage Software Simulating Initial Slider Linkage Concept

While the slider had several good qualities there are also many possible issues with it. The most pressing issues are as follows: The addition of a failure point, the addition of a wearing surface, The addition of a pinch point, and the geometrical challenges of achieving an acceptable range of motion.

After considering the initial slider linkage, we were able to see that the concept was sound and fairly applicable to our case. Using the same basic concepts, we altered the geometry to move the slider link from its previous position (vertically aligned with the position of the torsion rod) to a position where it vertically aligned with the tangent to the torsion rod input link path. This concept is shown in Figures 13a and 13b. Using a whiteboard for initial concept drawings, then a linkage software, we were able to sufficiently model the motion paths of each link in this mechanism.

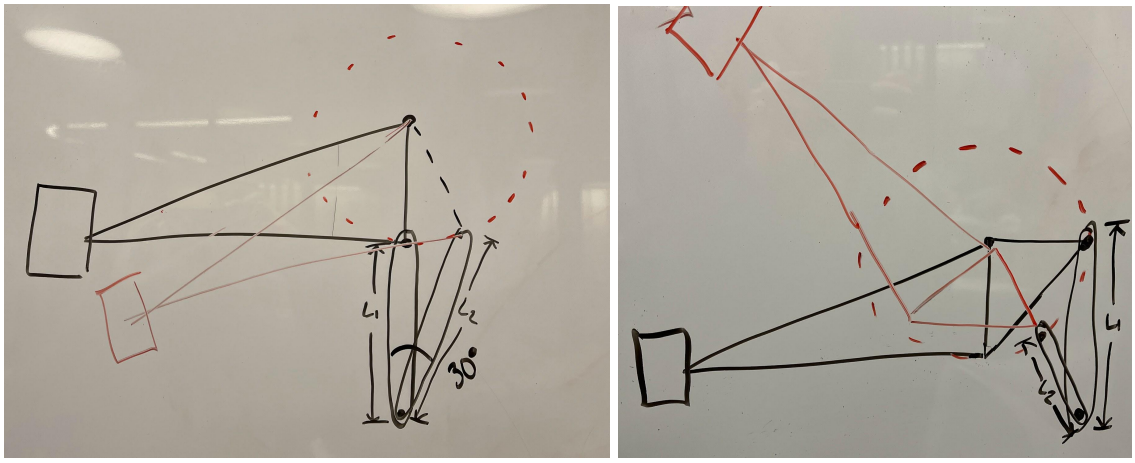

Figure 13a (left) Figure 13b (right): Conceptual Drawings of Position Change of Slider

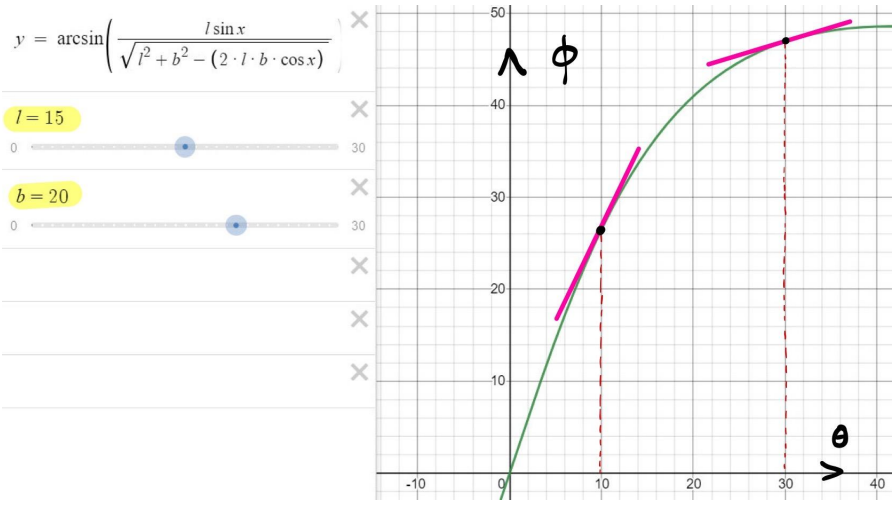

Figure 14: Graph of the Effect of Slider Link Lengths (l = 15 and b = 20) on Torsion Rod Velocity at Zero Travel (phi = 30) and Full Travel (phi = 10).

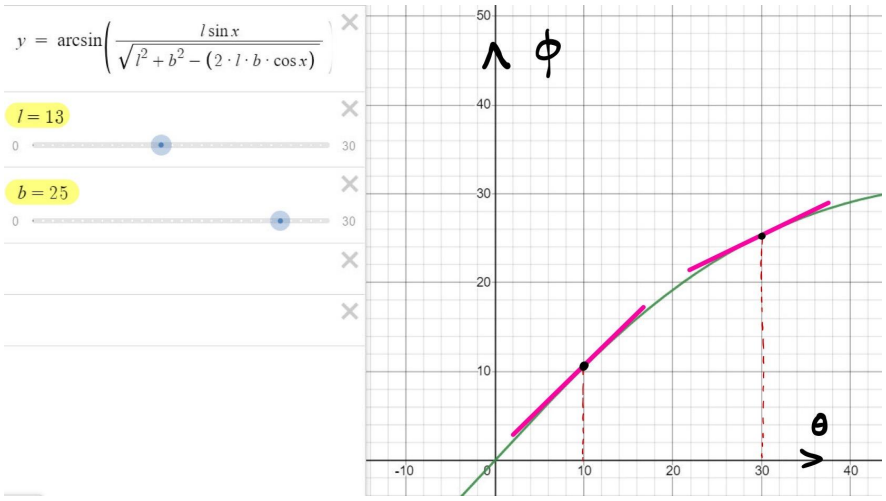

Figure 15: Graph of the Effect of Slider Link Length (l = 13 and b = 25) on Torsion Rod Velocity at Zero Travel (phi = 30) and Full Travel (phi = 10).

3.1.3.2 CAD Modeling and Additive Manufacturing

We then used CAD to parametrically model the linkage by defining all parts from the initial geometric sketch. This allows for changes in geometry based on form factor without changing the linkage input and output characteristics. For more information on this modeling strategy see methods section 3.5.1.

After 3D printing a preliminary mockup of this design, we were able to test it using the setup shown in Figure 16. To perform this test we took force measurements at 1 cm displacement intervals and plotted them to create a curve showing the relationship between reaction force and displacement of the suspension.

Figure 16: Slider Linkage First Iteration, Testing Setup

3.1.4 Slider Linkage Transfer Function

In order to relate the collected motor position data to an effector arm angular position, a transfer function between these two metrics was derived. Thus, the microcontroller can continuously read the motor position data to know when the suspension system is compressed and its location throughout the range of travel.

Method 1: Ideal Mathematical Model

Figure 17 illustrates the geometry and nomenclature used to create the transfer function.

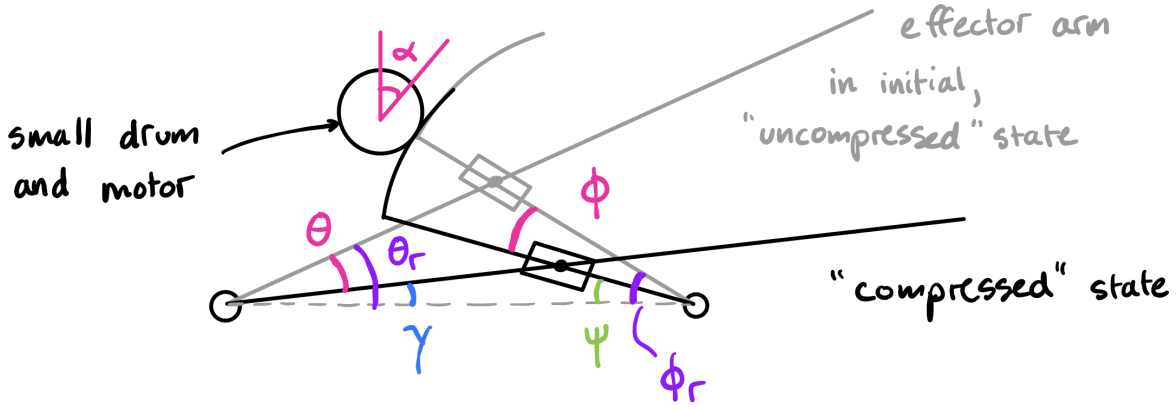

Figure 17 : Geometry Nomenclature for Motor Angle to Effector Arm Angle Transfer Function

The ratio and rolling interface between the small drum and the crust, the equation governing the relationship between the known α (motor angular travel) and ϕ (capstan and torsion rod angular travel)

Equation 3:

$$\alpha = 10 * \phi$$

ϕ_r and θ_r are defined as the resting angles between the pivot base segment and the capstan slider slot (51.38°) and effector arm (36.62°), respectively, when the suspension system is fully unloaded. Figure 18 highlights the geometry used to understand the relationship between ϕ and θ (effector arm angular travel).

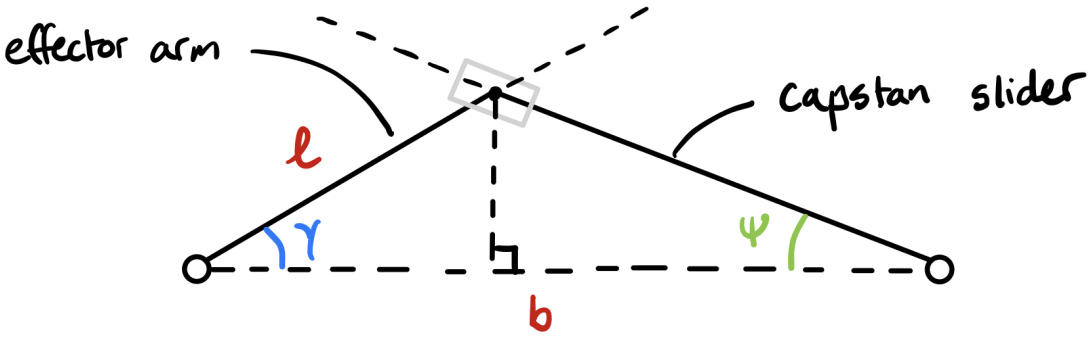

Figure 18: Geometry Used to Relate ϕ and θ

We applied a geometric analysis on the triangles with a shared edge using the law of cosines, shown in Eq. 5. This geometry is illustrated in Figure 18. Equations 4 through 6 show a system of geometric relationships used to relate ϕ and θ:

Equation 4:

$$\Psi = \phi_r - \phi$$

Equation 5:

$$\sqrt{l^2 + b^2 - 2 * l * b * cos(\gamma)} * sin(\Psi) = l * sin(\gamma)$$

Equation 6:

$$\theta = \theta_r - \gamma$$

We used a MATLAB symbolic solver to solving to populate arrays of the discrete relationship α and θ. We then applied a curve fit to these data to create a transfer function of θ with respect to α. This transfer function was used to post process the raw motor position data for determining the position of the effector arm during testing.

Method 2: Physical Model Data Collection.

To measure the relationship between the linkage and the motor, we created a test to measure the linkage and the motor angles at discrete points. Measurements were taken roughly every 5 degrees of the linkage arm and the digital readout attached to the linkage as well as the motor encoder value were recorded. The motor encoder data was shifted to account for not starting at zero due to slipping from previous testing. This data was plotted and a function was generated to calculate the linkage arm angle from the motor angle.

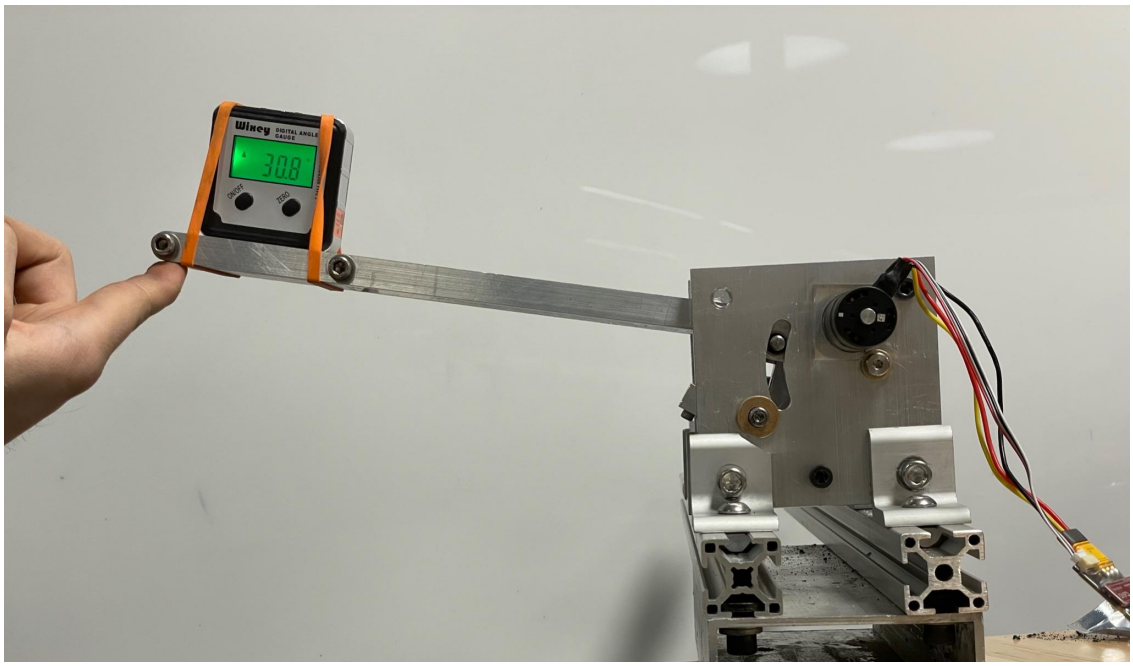

Figure 19: Testing the relationship between the linkage arm angle and the motor angle.

Refer to 4.1.4 for the results of the two methods used to create a slider linkage transfer function.

3.2 Capstan

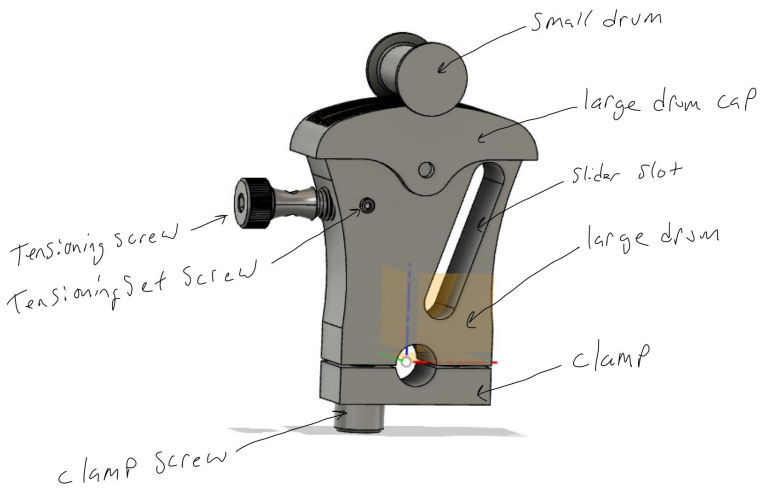

Figure 20: Capstan Nomenclature

3.2.1 Small Drum

3.2.1.1 CAD Modeling and Additive Manufacturing

The small drum was modeled primarily with a revolve that makes the cylinders and bores followed by a helix that traces out the path for the Dyneema and a swept cut of a circular thread profile. The motor shaft hole was bored out to 6.35mm on a 6mm shaft to make up for misalignment issues between the mounting plates that was causing the motor to bind. This extra clearance acts like a flex coupler to absorb slight misalignment.

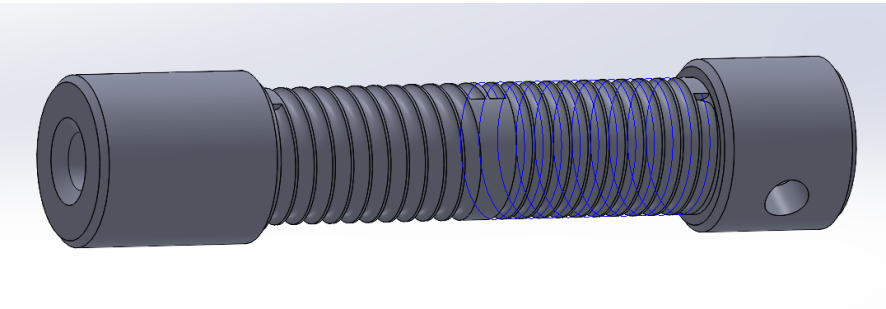

Figure 21: CAD Model of Small Drum for Capstan Assembly

The initial conceptual prints to test the design were 3D printed on a Formlabs 3L using Tough 1500 resin. These prints informed decisions about the depth of grooves, coil angle, and alignment factors. When creating test assemblies with the large drum of the capstan, we used the same method and material to print, but altered some design choices based on the conceptual prints.

We printed multiple iterations of the small drum using Tough 1500 resin on the FormLabs 3L printer with small changes to account for changes in the overall assembly of the suspension system. Once printed we developed methods for wrapping the Dyneema that account for the full range of rotational motion of the small drum.

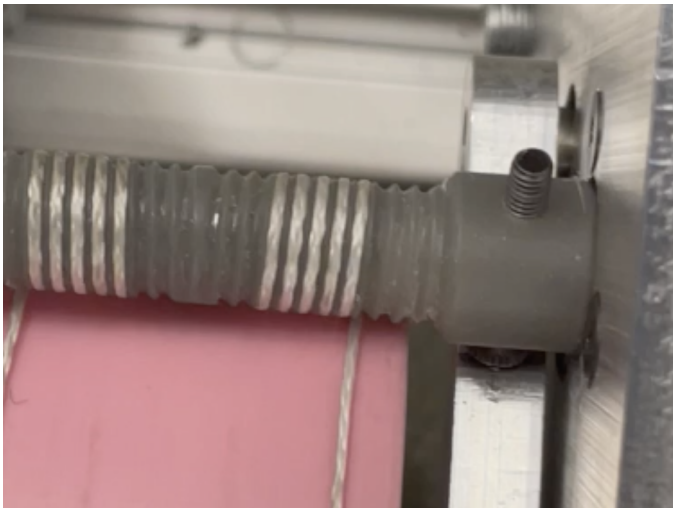

Figure 22: Resin Printed Small Drum

3.2.1.2 Machining

We manufactured two prototypes for the small drum from aluminum stock using a manual lathe. The first prototype had the same geometry as our resin printed small drum, but had better strength properties due to the material change. The second prototype had the same geometry but without grooves to guide the Dyneema around the drum. We chose to proceed with the smooth drum iteration as an experimental test to see how necessary the groves were to the function of the capstan.

In order to be left with a small drum with the least hop possible, all possible operations were done without refixturing the part. First he stock was fixtures with enough stick out to machine all features required. Then the front of the aluminum was faced, drilled, and reamed with the motor shaft fit. A live center was then fitted to the end and the small drum was roughed out. The threads were made with a custom grounded tool with a round profile that also made the well in the center. The threading mode on the lathe was used with 18 tpi being chosen as it is closest to our desired threading, the part was threaded slowly in both directions terminating at the center. The part was then parted at the end and re-fixtured backwards to be refaced, drilled, and tapped 10-32 for the shoulder bolt.

3.2.1.3 Combination Machining and Additive Manufacturing

We created another testing prototype for the small drum using a combination of additive manufacturing and machining. Because of issues with slip on the grooved surface of the aluminum small drum, we decided to proceed with the resin surface of the drum due to frictional properties with the goal of eliminating slip from the system. This prototype also included an aluminum core to prevent bending and binding in the system. Figure 23 shows the prototype below.

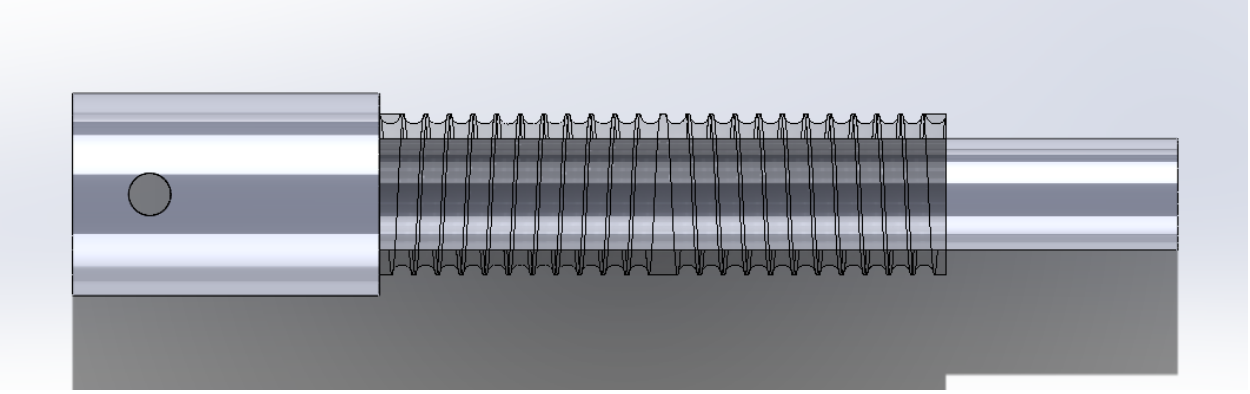

Figure 23: CAD Model of Hybrid Drum

The aluminum core model was based on the previously machined aluminum small drum with grooves, but the geometry changed slightly to accommodate the grooved resin sleeve. The collar with the hole for the motor shaft was extended to accommodate for the change in diameter of the aluminum shaft to avoid drilling through the shaft. We also removed the wider section of the shaft on the opposite side from the motor to allow the resin sleeve to slide into place. We fixed the resin print to the shaft using superglue.

The aluminum core was machined using a manual lathe. The process was very similar to the one used before, however, this time no threading was needed. The fastest speed the lathe was capable of was used for the final spring pass on the shaft in order to achieve the smoothest surface for a press fit. The resin sleeve was printed out of Tough 1500 and the center hole was reamed using the manual lathe for a precise slip fit on the aluminum core.

3.2.2 Large Drum

3.2.2.1 CAD Modeling and Additive Manufacturing

The initial design of the capstan system included a 30 degree wedge shaped large drum due to the limited travel of the torsion bar. Through iteration in the CAD model, the large drum was modeled into a hook shape to make room for the pivot of the linkage arm. We decided to move the linkage arm pivot to make room for the full stroke of the capstan. This allowed us to make the large drum into a rectangle. After discussing the manufacturing of the large drum, we separated the large drum into the main body and the crust to allow for easier iteration of the surface that the cable interacts with. The large drum was also modified to account for the new tensioning system (see section 3.2.4.3)

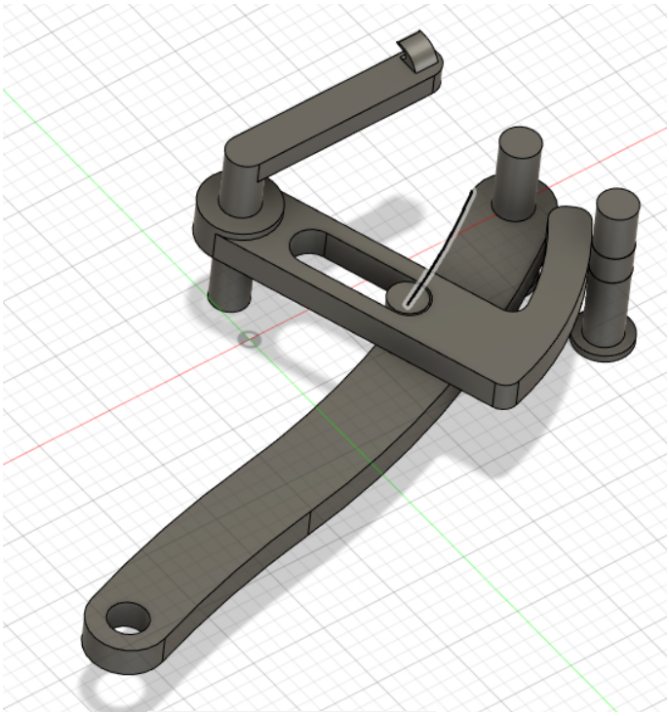

Figure 24: Low volume Capstan Iteration, Initial Concept

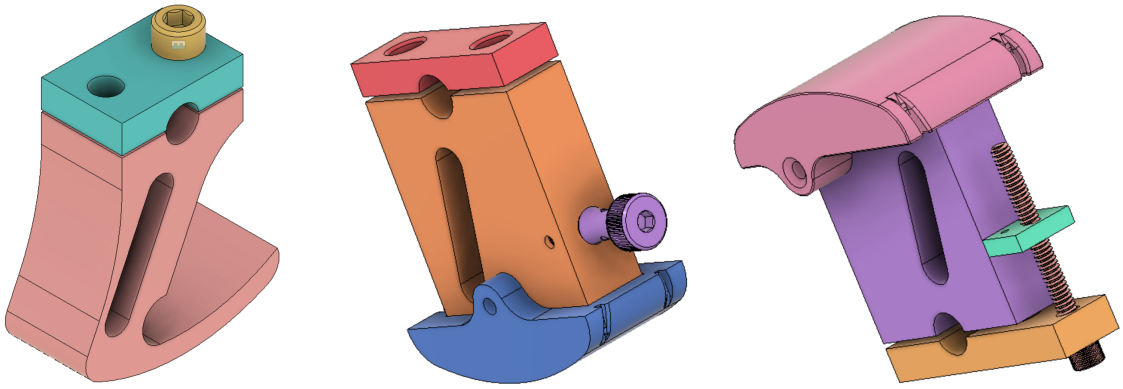

Figure 25: Evolution of the Large Drum Assembly

3.2.2.2 Machining

We used a CNC mill to machine this piece. We used a 2”x2”x1” piece of aluminum stock to fabricate the part. First, we drilled the torsion bar hole to ensure precise sizing. The rest of the part was then milled with an endmill.

3.2.3 Crust

3.2.3.1 CAD Modeling

Using CAD, we designed the crust for the large drum to fit over the large drum and have slots for the cord to loop around the top face of the crust for the purpose of being able to have a double wrapped small drum while only needing to tenison one cord. The model was created with the intent to closely fit around the top face of the large drum. It was also designed to be fully replaceable and easy to manufacture. The reasoning for making the crust replaceable is to allow for adjustability. By changing the input parameters, we can easily redesign a new crust with a larger or smaller angular section to accommodate a change in the torsion rod specs. Figure 26 shows the cad model for the crust component.

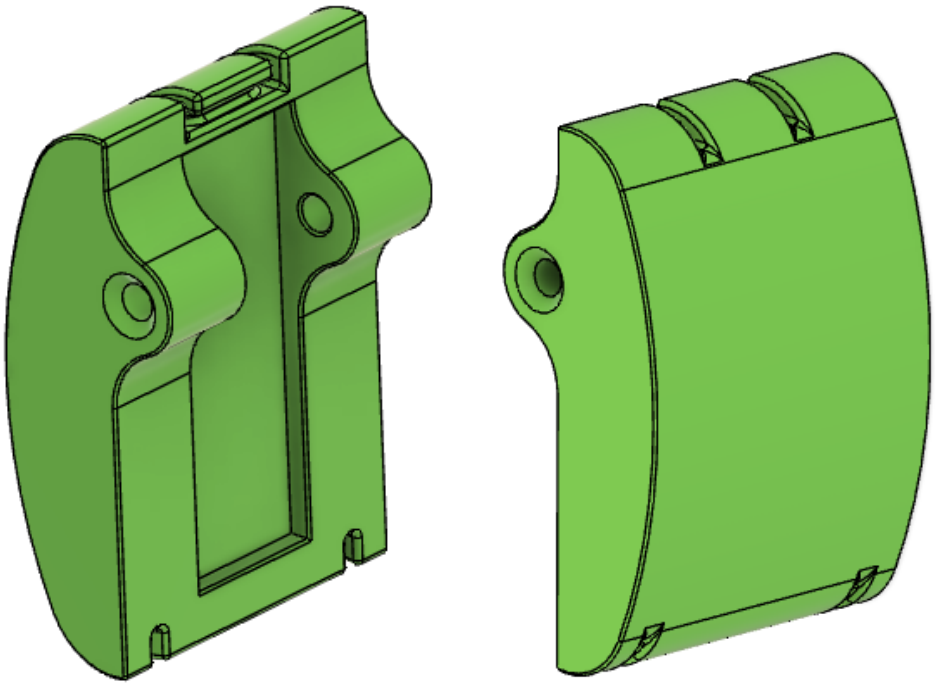

Figure 26. CAD Model of Crust

3.2.3.2 Additive Manufacturing (Conceptual Print)

For proof of concept, we printed the crust component using a Prusa i3 and PLA. Once manufactured, we were able to assemble this component with a print of the small and large drums, held together using 6-32 screws and the Dyneema® cord, shown in Figure 27. By assembling all of the components we were able to observe the interaction between the parts and make any necessary adjustments for better fit.

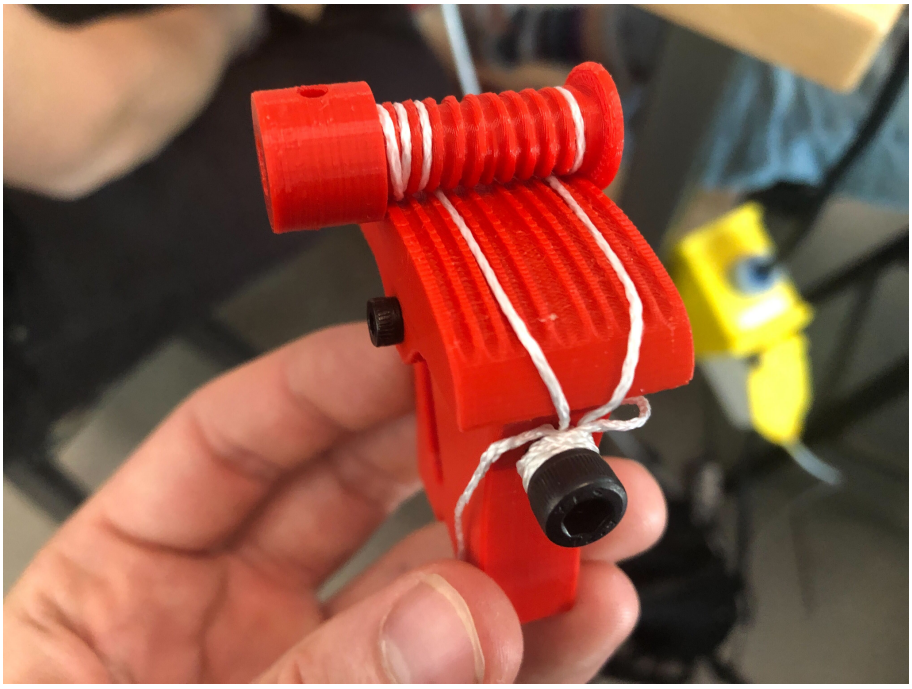

Figure 27: Assembled Version of Conceptual Prints

3.2.3.3 Additive Manufacturing (Resin Print)

For the final assembly we chose to print the crust component from Tough 1500 In the FormLabs 3L resin printer. We chose to print with resin because of its strength and the quality of the print compared to using the traditional PLA. The resin printer, however, requires a few extra steps including isopropyl alcohol baths, trimming supports and curing after printing. Once fully cured we used a chisel to remove the remaining lumps of cured resin leftover from the supports. This allowed for a better, more snug fit on the large drum. The print was then fastened, again using M3 screws.

3.2.4 Tensioner Systems

3.2.4.1 Guitar Peg Tensioner

In our first few iterations for printing parts for the capstan, we chose to use a guitar tuning peg in the assembly. Because of the similarities between the intended use of the tuning peg and our application (tensioning the cord that wraps around both the small drum and the crust component), we were able to easily apply the same tensioning concept to the project.

To assemble the capstan component, we wrap the cord around the small drum, follow the channel hook on the crust to come back and wrap the small drum in the opposite direction. To tension the cord, we insert both ends through the hole in the shaft of the peg and twist the peg multiple times to secure the ends. The pressure from the wrapped cord secures the end of the cord in the hole. The guitar tuner also allows for variable tension by twisting the peg.

3.2.4.2 Shoulder Bolt Tensioner

After testing the concept of a rotational tensioner for this application we proceeded to conceptualize and machine a shoulder bolt to be used as our tensioner. We used a manual lathe to cut the contour shown in Ffigure 28 and used a manual mill to drill the hole through the center of the shoulder bolt. This tensioner was then screwed into the tapped hole on the large drum and secured with an M3 set screw. The same method as stated in section 3.2.4.1 was used for tensioning the cord.

Figure 28: Shoulder Bolt Tensioner

3.2.4.3 Linear Tensioner

For the final iteration of the test setup, we created the tensioner shown in Figure 29. We machined the tensioning plate by manually cutting out the outer shape and drilling the three holes for the strands and the tensioning screw. Both strands from the capstan were threaded through the tensioning plate holes and tied using a figure eight knot to fix the strands together. To ensure the ends of the strands would not fray and compromise the knot, we applied small amounts of superglue to each cut end.

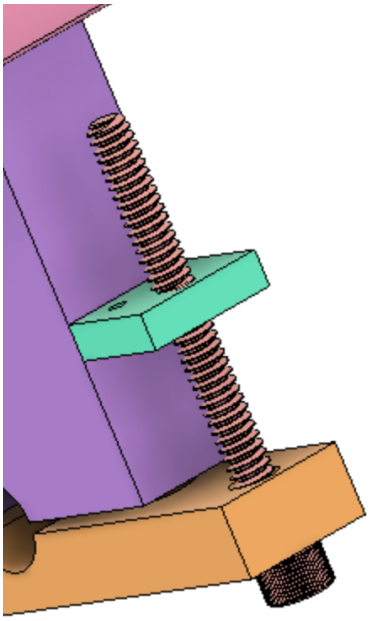

Figure 29: Linear Tensioner

3.3 Torsion Rod Spring/Clamps

3.3.1 Knurling Operation

Using a manual lathe and a crosshatched knurling tool, we performed the forming operation at either end of the torsion rod. Because of the lateral pressure on the rod from the tool while spinning in the lathe, we used a spot drill to create a small hole on the opposite face of the rod. This hole was used to insert a live tailstock for additional support of the rod while the forming operation took place. The knurling operation took place at 80 rpm.

3.3.2 Testing

We performed a second slip test on a steel rod for proof of concept and ensured the combination of our clamp design and the knurled surface had enough friction to prevent slip to a reasonable degree. We chose to test on steel because of the availability and cost of this material compared to titanium. Once deciding on the dimensions of the test rod and performing the knurling operation, we adjusted our initial clamp CAD models to create a clamp suitable for use in testing.

The clamps in our suspension test rig were designed as two rectangular components with a semicircular hole drilled into one face to hold the rod. The holes are slightly undersized to ensure complete contact and a “squeezing” effect on the rod. Additionally, the clamps have tapped holes with a 1in separation to fasten both pieces together. These holes were tapped to accommodate ¼ 20 screws because of their strength and size characteristics.

After doing a rough cut with a band saw on the 1 inch thick stock, the test clamp was faced using a Bridgeport manual mill with a 2in facing mill. The hole for the torsion rod was

then drilled by first, spot drilling and creating a pilot hole, then drilled using a size O bit. The Screw holes were also drilled using the manual mill and #7 bits, then tapped manually with a ¼-20 tap. We then knurled the steel rod on one end and cut the other to create a tab like section to be able to clamp with a wrench for the slip test.

After machining and assembling the steel rod and clamp, we used a vice and aluminum plate to secure and stabilize our test setup. Next, we attached a 13.5” adjustable wrench to the cut end of the rod and attached a spring scale to the end of the wrench. We marked the rod and clamp using the same method mentioned in section 3.3.1, and pulled on the spring scale to measure the maximum force applied to the end of the wrench. We performed two tests, both on a knurled and smooth portion of the steel rod. Using this data we were able to see if the rod slipped and at what torque it slipped. Figure 30 shows our slip test setup.

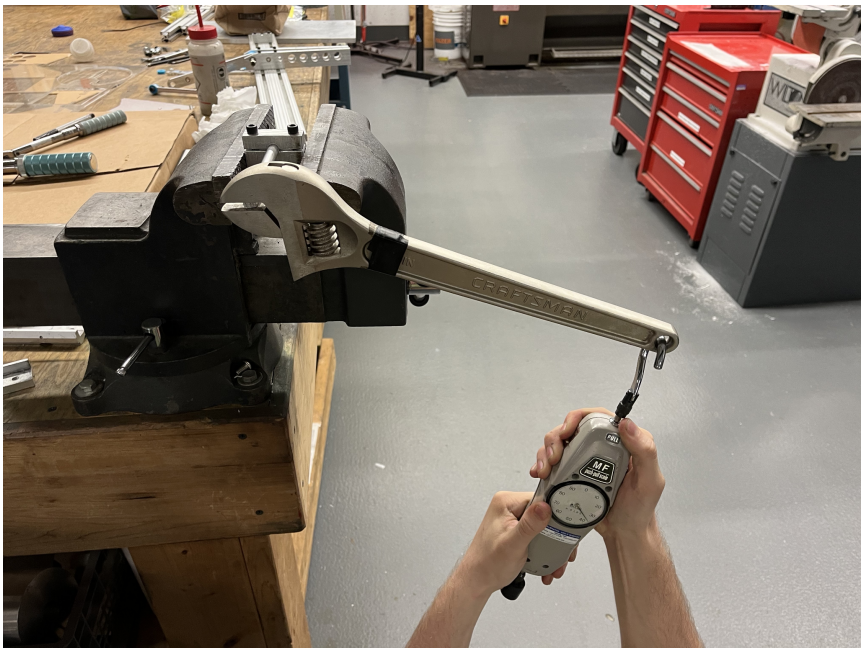

Figure 30: Steel Rod Slip Test Setup

3.4 Motor

3.4.1 Activated Damping

To perform initial testing on the motor, we built a test fixture that would apply a spring load to the end of a moment arm to simulate the torsion bar. This arm would be actuated by hand to simulate the response of various control algorithms. The results of this test were assessed tactically to gain an intuitive sense of how different models feel. This test was designed to influence decisions later about how to program the damping system.

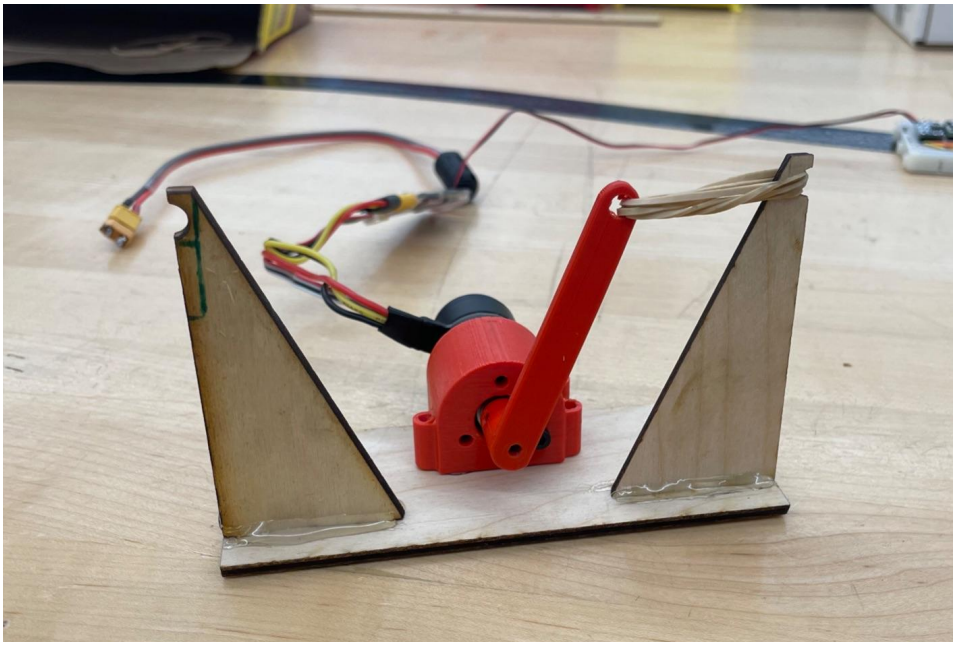

Figure 31: Active Damping Motor Test Fixture

3.4.2 Regenerative Damping

To test the regeneration power of this motor, we attached the output of the motor to a three-phase rectifier which was boosted to above the cell voltage of the battery with a boost converter. The power was directed into a battery to charge it. We ran this test at a medium speed for one minute and measured the voltage increase of the battery.

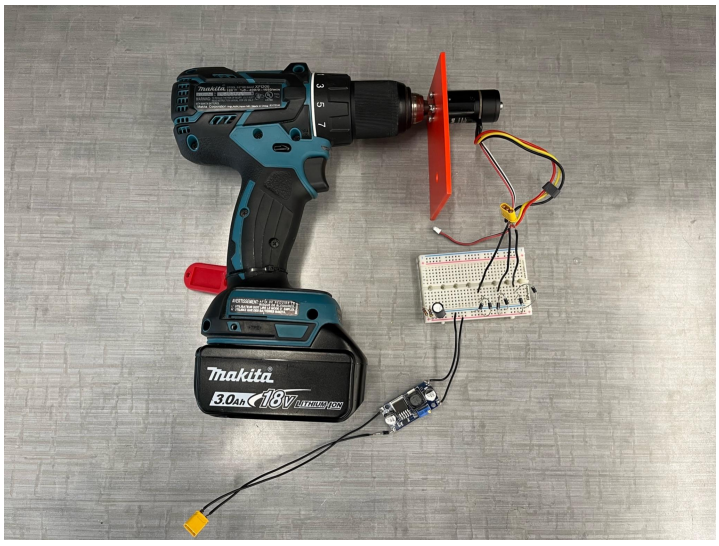

Figure 32: Drill Power Regen Test Setup

3.5 Assembly and Testing

3.5.1 Skeleton CAD Modeling Strategy

Since our design includes many parts with shared geometries it was necessary to find a robust CAD workflow in order to be able to make changes in the future. The tactic we settled on is called skeletal modeling. We utilized this by housing most relations on a single skeleton file that was imported into every assembly file with one assembly per rigid group. This skeleton file contains sketches that detail the position of each component in relation to each other as well as planes to extrude between, axis for assembly to assembly mates, and other such geometry that can be used to relate the different components.

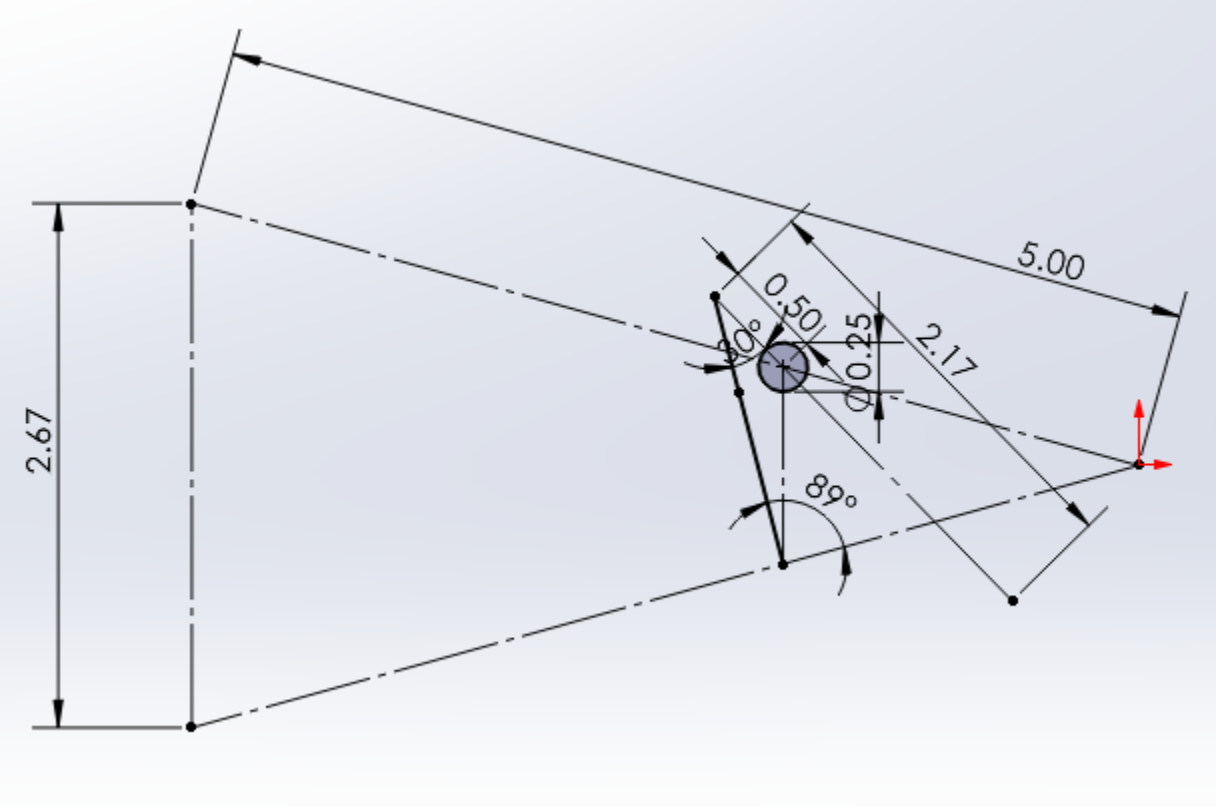

Figure 33: Geometry Sketch From Skeleton File

The first sketch made in the skeleton file is shown in Figure 33, it defines our base geometry for many other components. From this sketch the length of links, distance between mounting holes, and the length and position of the capstan sliding linkage can be determined.

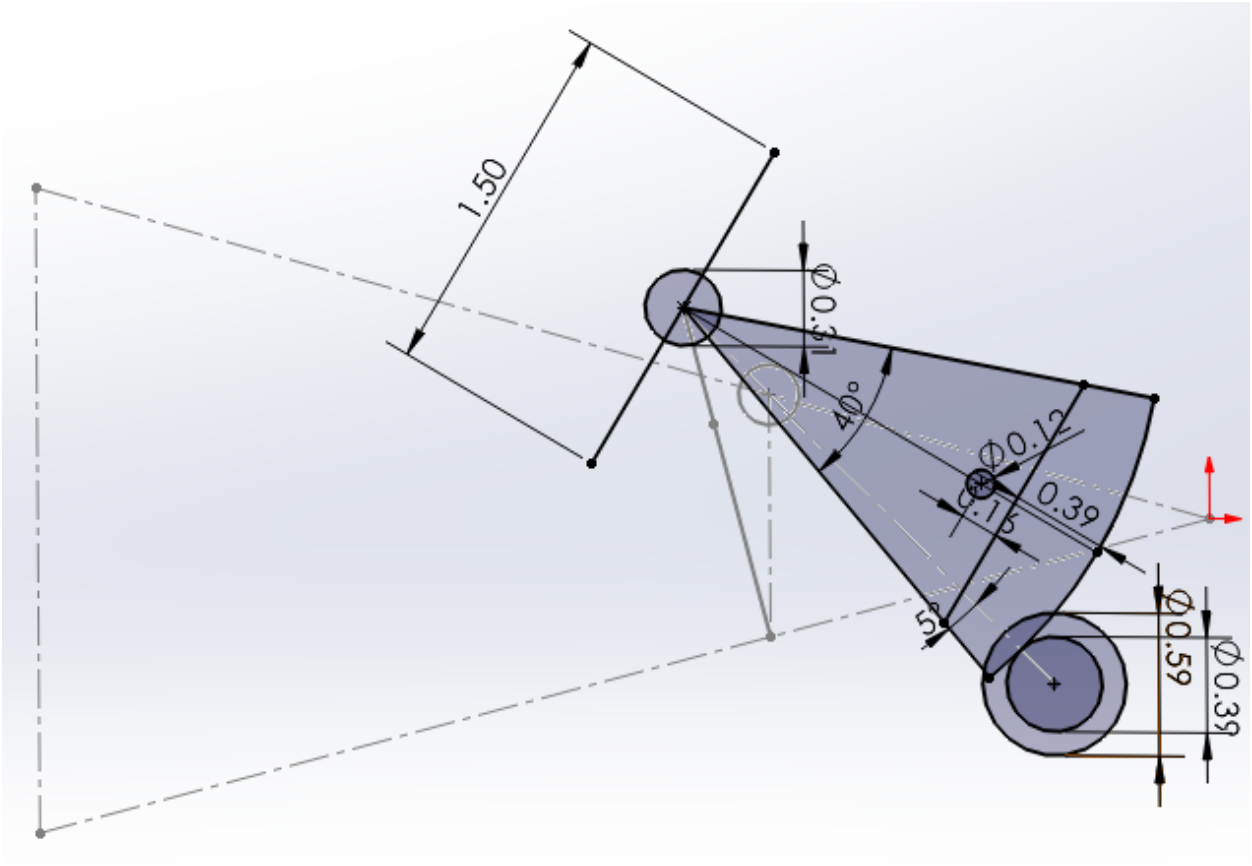

Figure 34: Skeleton Sketch for Capstan

From that initial sketch we build out to a skeleton sketch for the capstan that defines its geometry more fully, shown in Figure 34. This sketch relates to the previous and adds extra capstan dependent features. This geometry is in the skeleton file as it is referenced in multiple capstan relating components like the large drum, crust, and clamp. This whole skeleton part is imported into every subassembly that defines each rigid group.

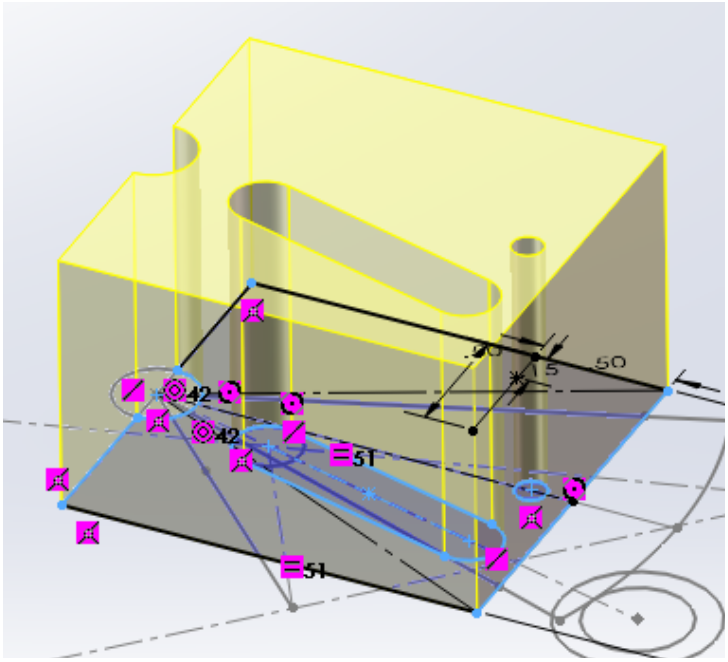

Figure 35: Capstan Large Drum extrusion Sketch

The relations in the sketch defining the main body of the large drum are shown in Figure 35. All relevant geometry is contained on the skeleton file. This way if large scale changes to the whole mechanism's geometry must be made the file does not break. This level of skeleton part utilization is continued to the assembly level with the location of the capstan in the main assembly being defined by an axis at the torsion rod where it rotates.

3.5.2 Assembly

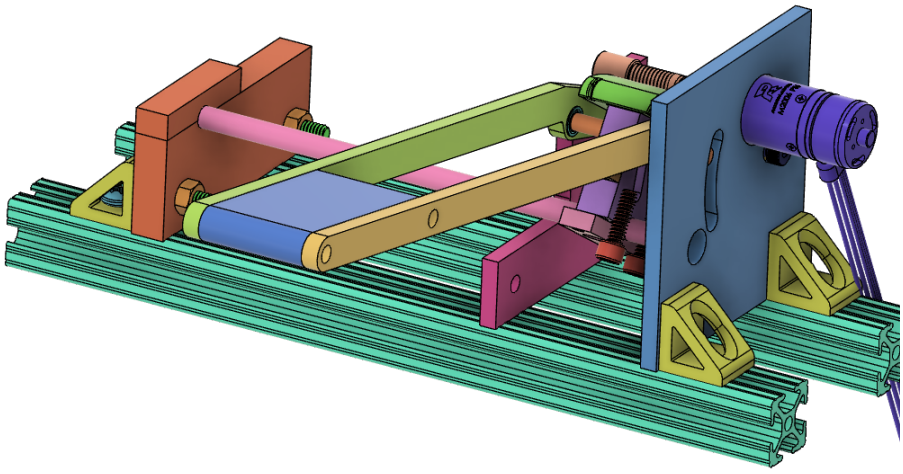

Figure 36: Full Assembly CAD

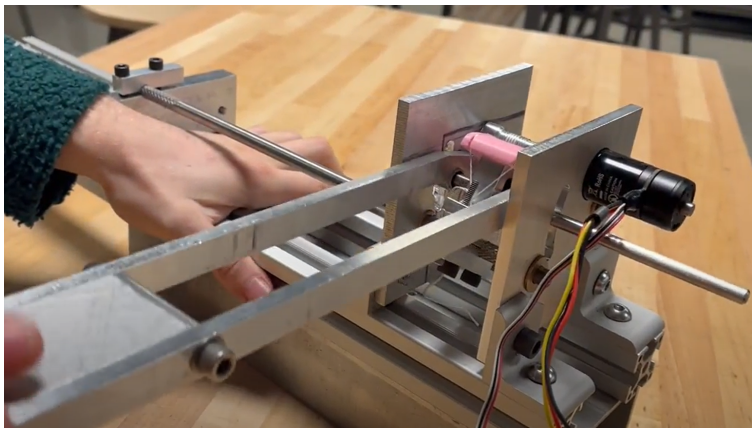

Figure 37: Full Assembly

In the full assembly, 1.5 inch t-nut aluminum extrusions were used as they allow for significant adjustment and iteration without the need for machining new mounting plates. The aluminum extrusion mounting brackets decided the mounting hardware as 5/16"-18. This choice became problematic when the 8020 did not provide the stiffness needed for testing, this problem was easily remedied by bolting aluminum rectangular tubing to the bottom. Additional stiffness came in the form of standoffs between the two plates as shown below.

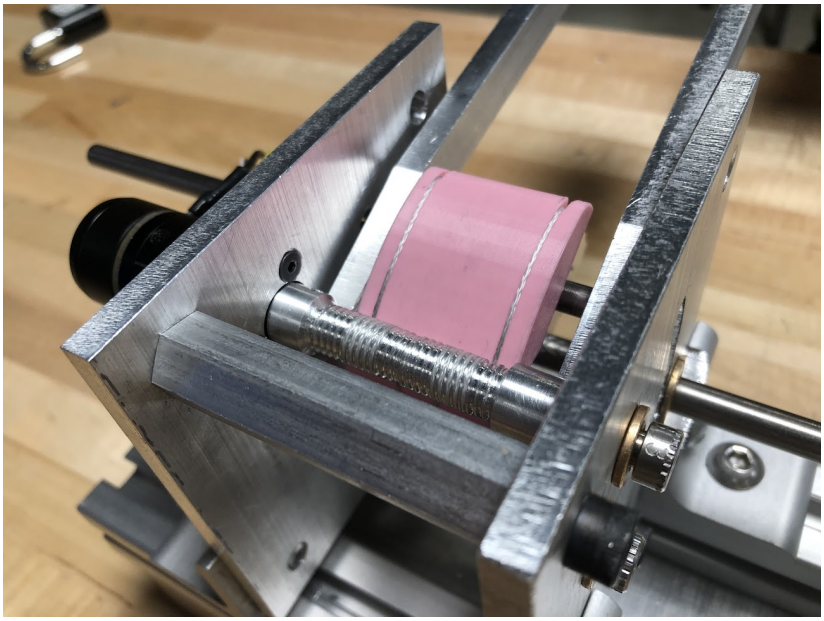

Figure 38: Standoff Between the Two Mounting Plates

3.5.3 System Response Testing

To perform this test, we secured the suspension fixture to a rigid table and secured the torsion rod with the linkage at the middle of its travel. This reduced the load on the system during the tests to minimize errors due to the cable slipping on the small drum and deflection in the system. Attaching the torsion rod at this position caused the linkage to sit at roughly 40% of its travel which simulates the preload of a rider standing on the skateboard. The linkage arm was

pulled down with 100N of force which brought the linkage arm to roughly 70% of its travel. The system was then released and the response was recorded through the motor encoder.

We repeated this test at damping scale factors (0, 2.5, 5, 10, 25, 50) to model the system response at different damping coefficients. The damping of the motor is controlled with a closed loop control algorithm based on the motor velocity and the scale factor. Each test was normalized to start at the same value to account for slip during each test. To model the response of the linkage arm, we passed the motor data through the transfer function (see section 4.1.4).

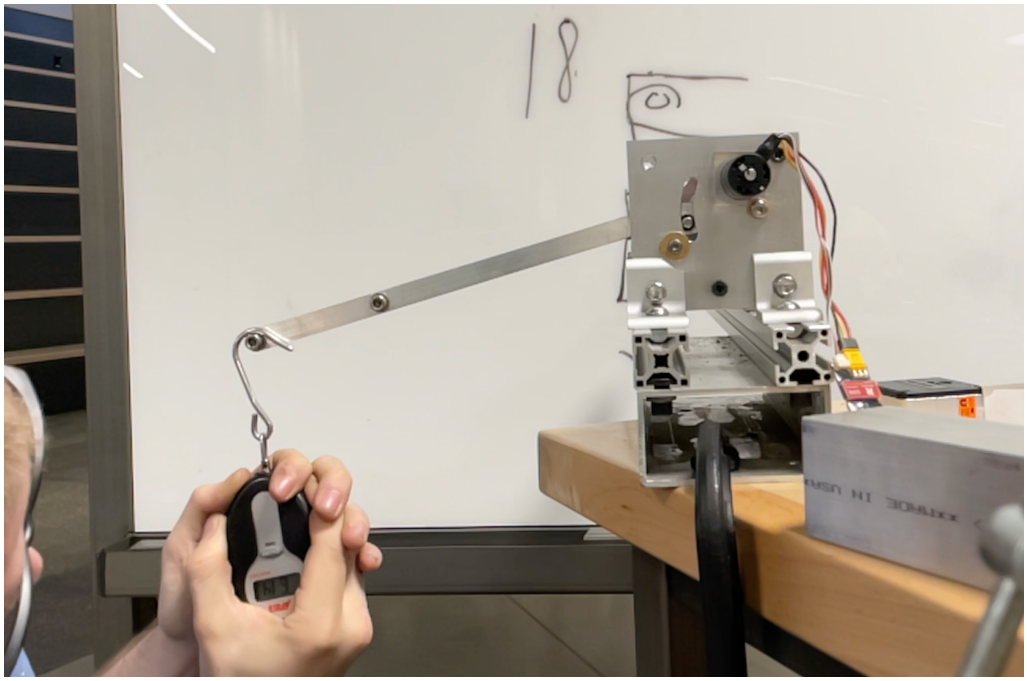

Figure 39: System Response Test Setup

3.5.4 Motor power regeneration testing

Using a three-phase rectifier, we measured the voltage output of the motor from an oscillating input of about 1Hz. The output of the three-phase rectifier was connected to a resistor and an oscilloscope to measure the output.

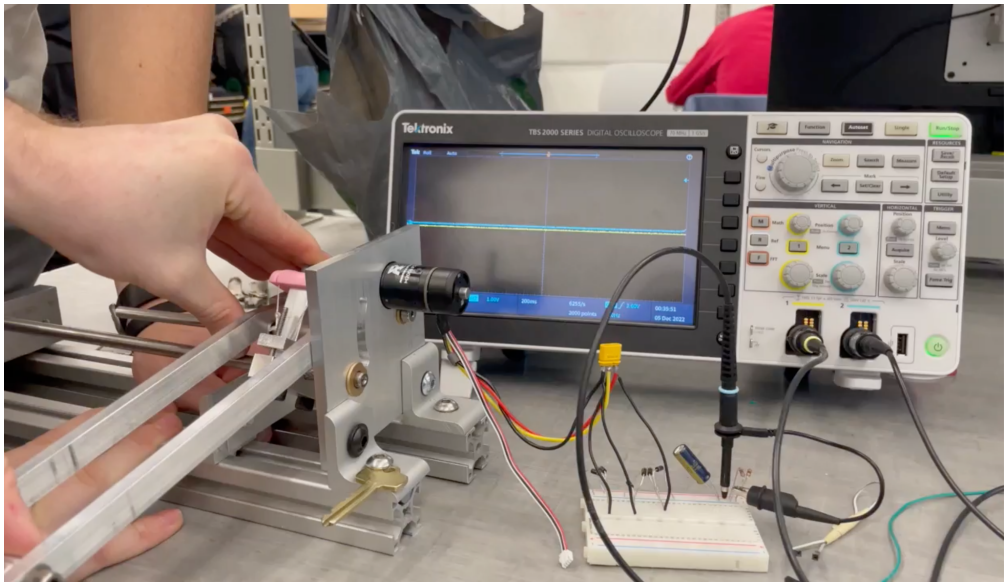

Figure 40: System Oscillation Voltage Testing

To test the power regeneration of the motor at different speeds we created a test fixture to drive the motor at constant speeds and measure the voltage increase of the battery. Each speed was tested for two minutes and the voltage increase was measured at the end of the two minutes.

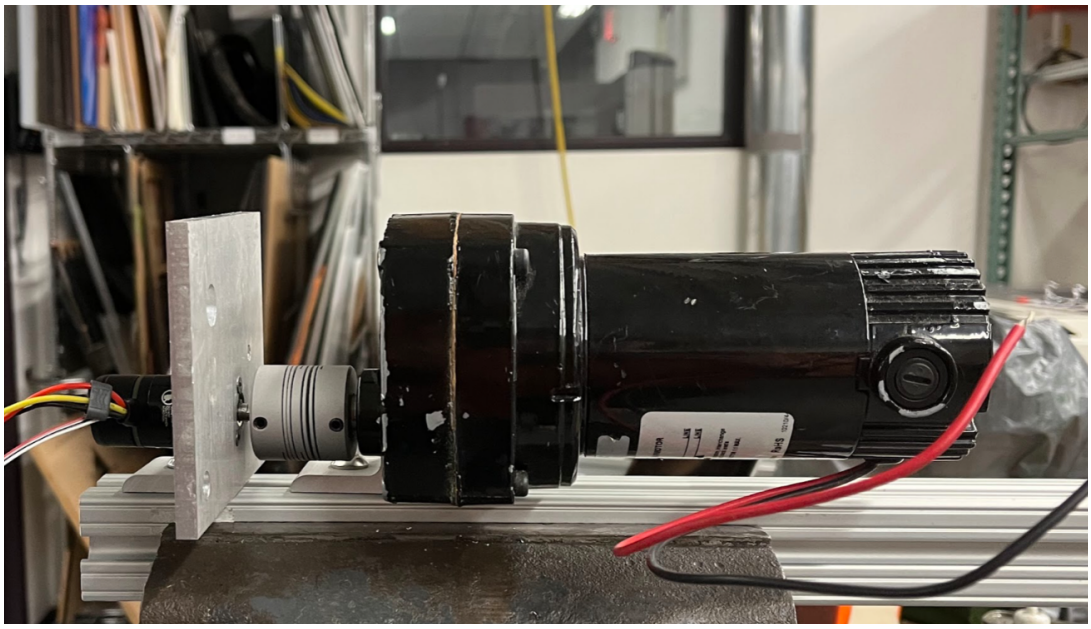

Figure 41: Battery Regen Motor Speed Test

4 Results and Discussion

4.1 Linkage

4.1.1 Perpendicular Linkage

In the first demonstration, we changed the position of the wheel link from 10” to 9 ½”. From this we can see that the initial angle of the torsion rod link (wheel is still at 10”) is 3 degrees below horizontal. After moving the wheel link up to 9 ½”, the angle of the torsion rod link is 5 degrees above the horizontal, so a total of 8 degrees of movement was recorded when the wheel moved up ½”.

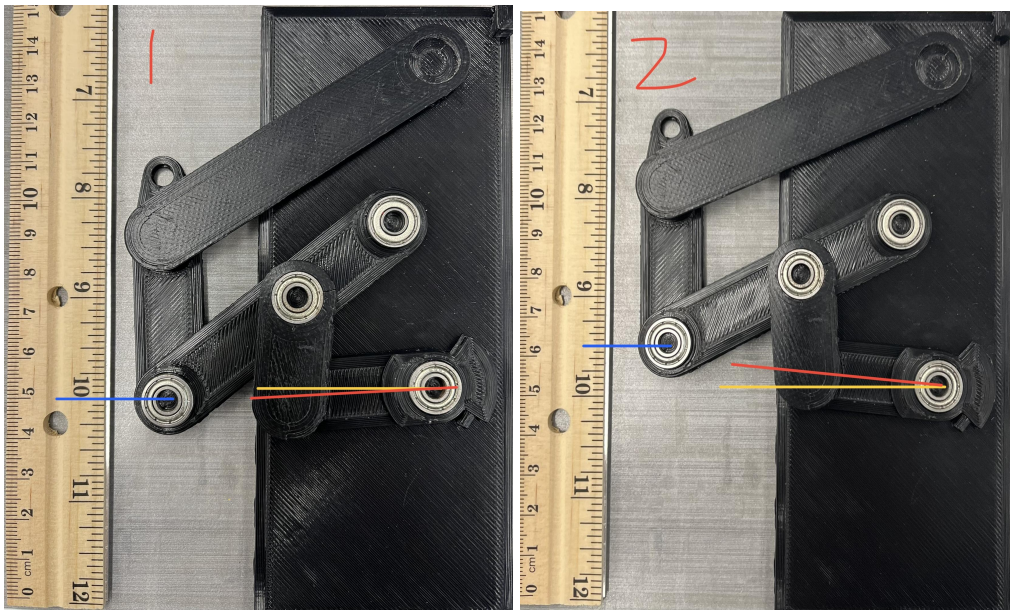

Figure 42 (left) and Figure 43 (right): Test Case 1 forPerpendicular Linkage Test

In the second demonstration, we change the position of the wheel link from 8 ½” to 8”. In this case the initial angle of the torsion rod link is 25 degrees and the final angle is 38 degrees. The resulting 13 degrees of movement proves the concept of a larger movement from the torsion rod link as the wheel moves through its stroke.

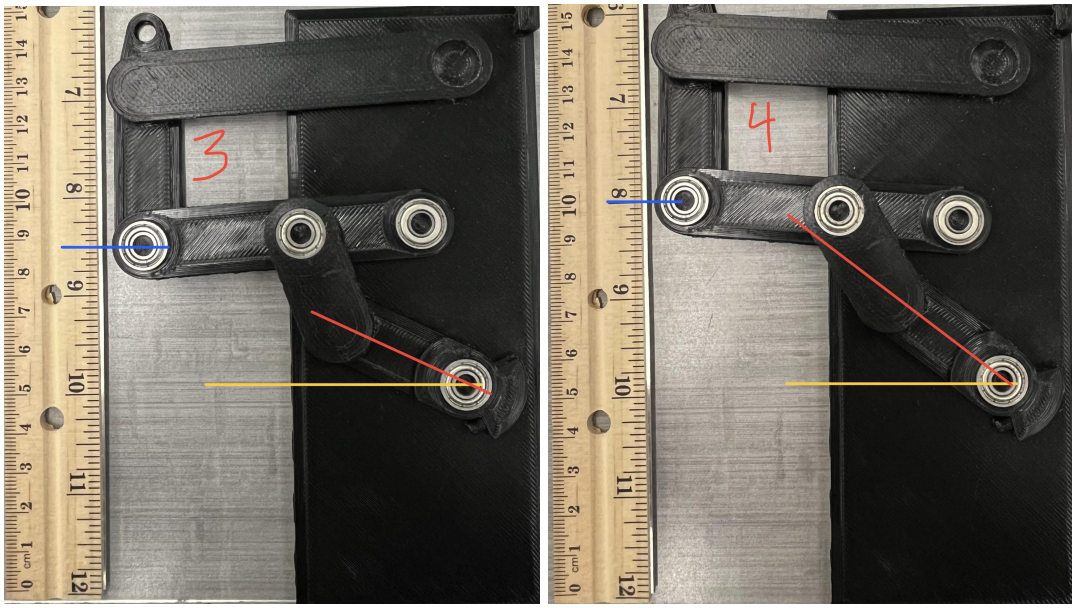

Figure 44 (left) and Figure 45 (right): Test Case 2 for Perpendicular Linkage Test

When analyzing the geometry of the linkage as it moves through the stroke, we can see that the input link pulls on the torsion rod link at a 90 degree angle. Later in the stroke when the linkage is "maxed out" the angle at which linkage A pulls on linkage B is much greater.

Equation 7, shown below, represents torque.

Equation 7:

$$\tau = rf\sin\theta$$

Where τ is torque, r is the distance at which a force is applied, f is the force applied and θ is the angle at which force is applied. Based on this equation, the decrease in angle throughout the stroke (when f and r both remain constant) decreases the torque applied to the torsion rod. This results in a decrease in reaction force from the torsion rod as the linkage travels to a maxed out compressed position.

Based on this data we concurred that this linkage was not fit for the purpose of amplifying the reaction force from the torsion rod as the stroke of the system continues. Because of this, we decided a slider linkage is still the best option.

4.1.2 Curved Slider Linkage

We discussed the concept of a curved slider to identify possible flaws in the design before proceeding. Although conceptually the idea was sound and could theoretically produce our desired results, the design was problematic due to the nature of sliders already having high likelihood of extreme wear in addition to the curvature of the path which would likely cause even more wear than usual. After consideration about the function of the slider and the likelihood of part failure due to binding, friction, and other undesirable loads, we decided to move on after CAD modeling without doing any physical iterations of the concept.

4.1.3 Slider Linkage Proof of Concept

The graph below shows the force required to depress the 3D printed suspension to the linear travel that the suspension makes. The linkage was tested with two different spring coefficients by adding more rubber bands. Two trials of each spring coefficient were used to ensure repeatability. The graphs are not linear and the force per unit of linear travel increases the more the suspension is depressed. This confirms the idea that the slider was doing what it was designed to do by increasing the force as the pin reached the center. One variable we were unable to account for was friction in the slider.

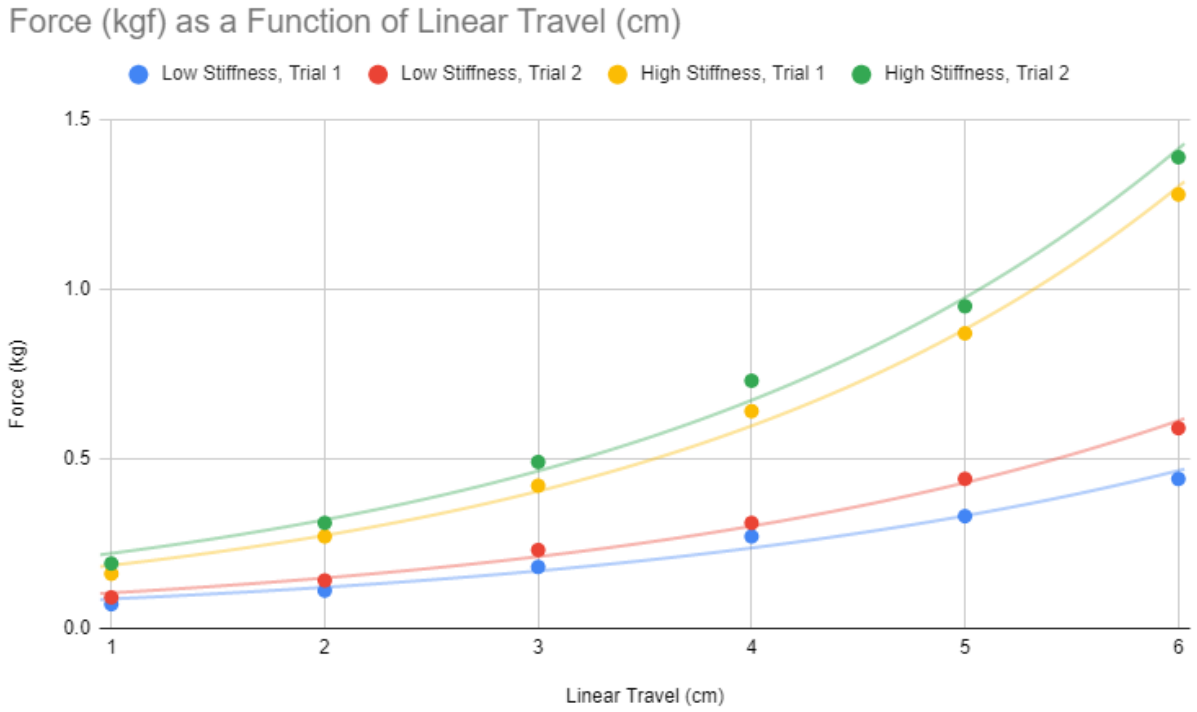

Figure 46: Spring Scale Test Results on Slider Prototype

4.1.4 Slider Linkage Transfer Function

Following the methods described in 3.1.4 Slider Linkage Transfer Function, we obtained the following results. Though 300 degrees of angular motor travel was assumed due to the capstan drive's 10:1 gear ratio, we observed only 210 degrees of motor travel with the microcontroller. This is likely due to backlash within the system, notably at the pinned interface between the small drum and motor shaft. Thus, we created a new discrete calculation where 30 degrees of effector arm travel correlates to 210 degrees of motor travel. The change in effector arm angle, theta, was solved at discrete steps of alpha from $0 < \alpha < 210$ degrees. Alpha and theta were stored in equal size arrays "motor_alpha" and "theta" for each 1-degree discrete value of alpha. These data were plotted in Figure 47 and fitted to a two-term power series model using MATLAB's Curve Fitter tool shown in Figure 48.

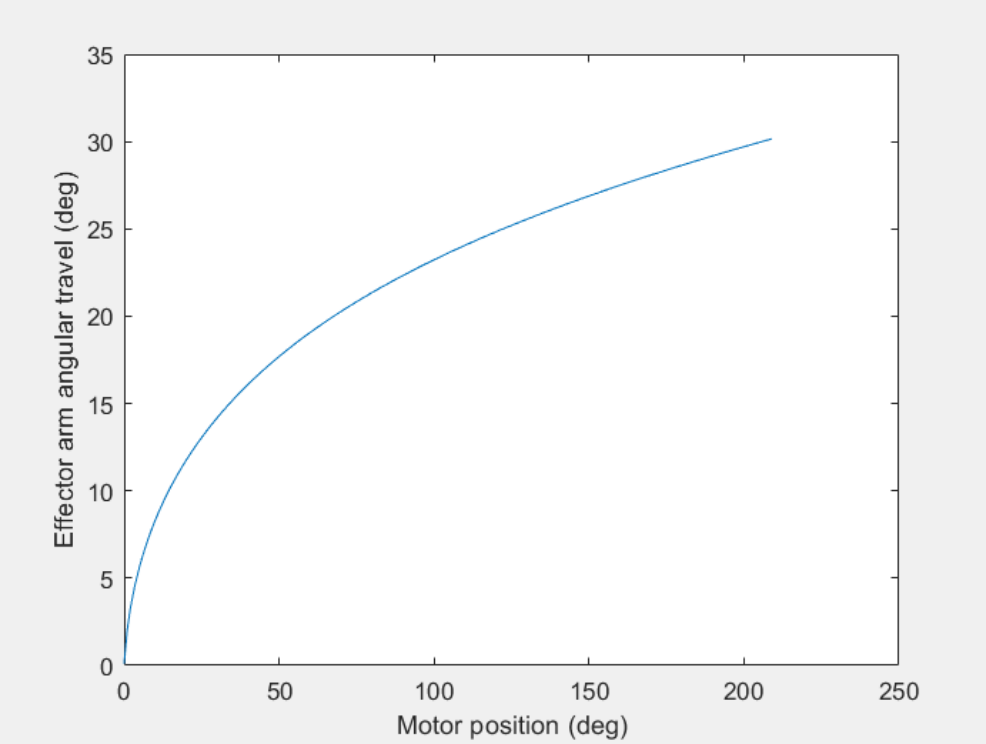

Figure 47: Effector Arm Angular Position as a Function of Motor Angular Position Readout

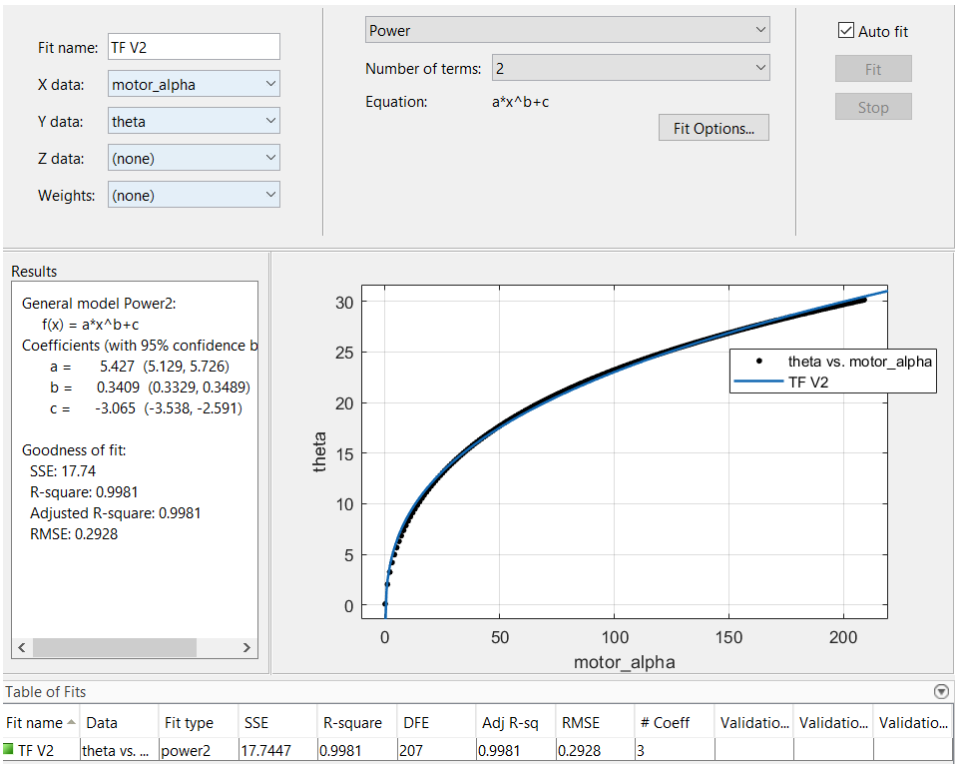

Figure 48: Applying a two-term power series curve fit to relationship between effector arm and motor angle

The curve fit is effectively a transfer function between α and θ. The function was integrated into the motor control script in order to know the position, or compression state, of the effector arm. Provided that the suspension system was powered on, and therefore zeroed, in a fully uncompressed state and assuming no deflection, slipping, or backlash within the system, this transfer function estimates the angle of the effector arm given a motor angular position. See Appendix 4.1.4 for the MATLAB script used in solving theta with respect to alpha using Equations 3, 4, 5, 6 and a discrete method.

We plotted the data and fit a power curve. The resulting transfer function from this test is very close to the transfer function that was calculated theoretically. The main difference is that the mathematically derived transfer function includes a y offset of the function. This offset is added to the mathematically derived one to fit the lower end of the data better. In the practical test we were experiencing that backlash was preventing us from measuring data precisely and that the uncertainty at the low end outweighed the accuracy of the models. The practical test confirms that the mathematically derived transfer function is an accurate model of the system given the backlash in the system.

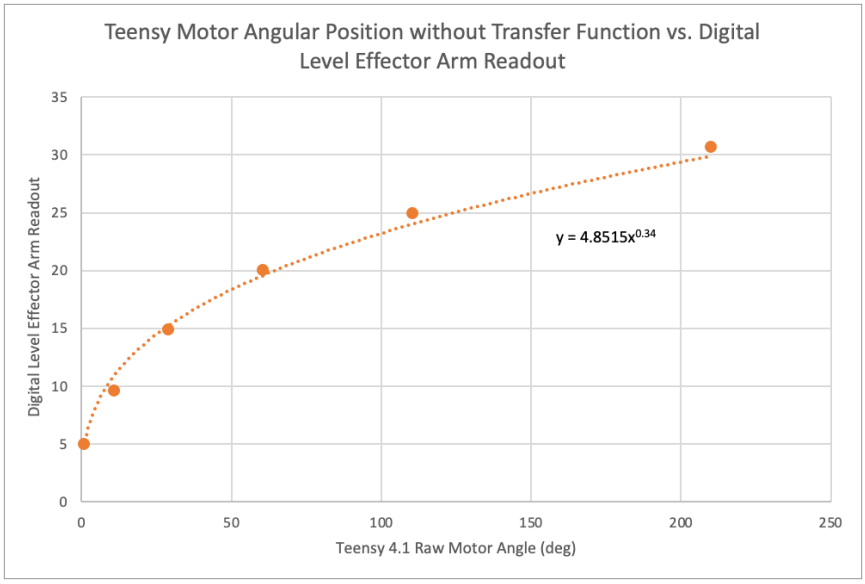

Figure 49: Data Collected from the Motor and Linkage Arm

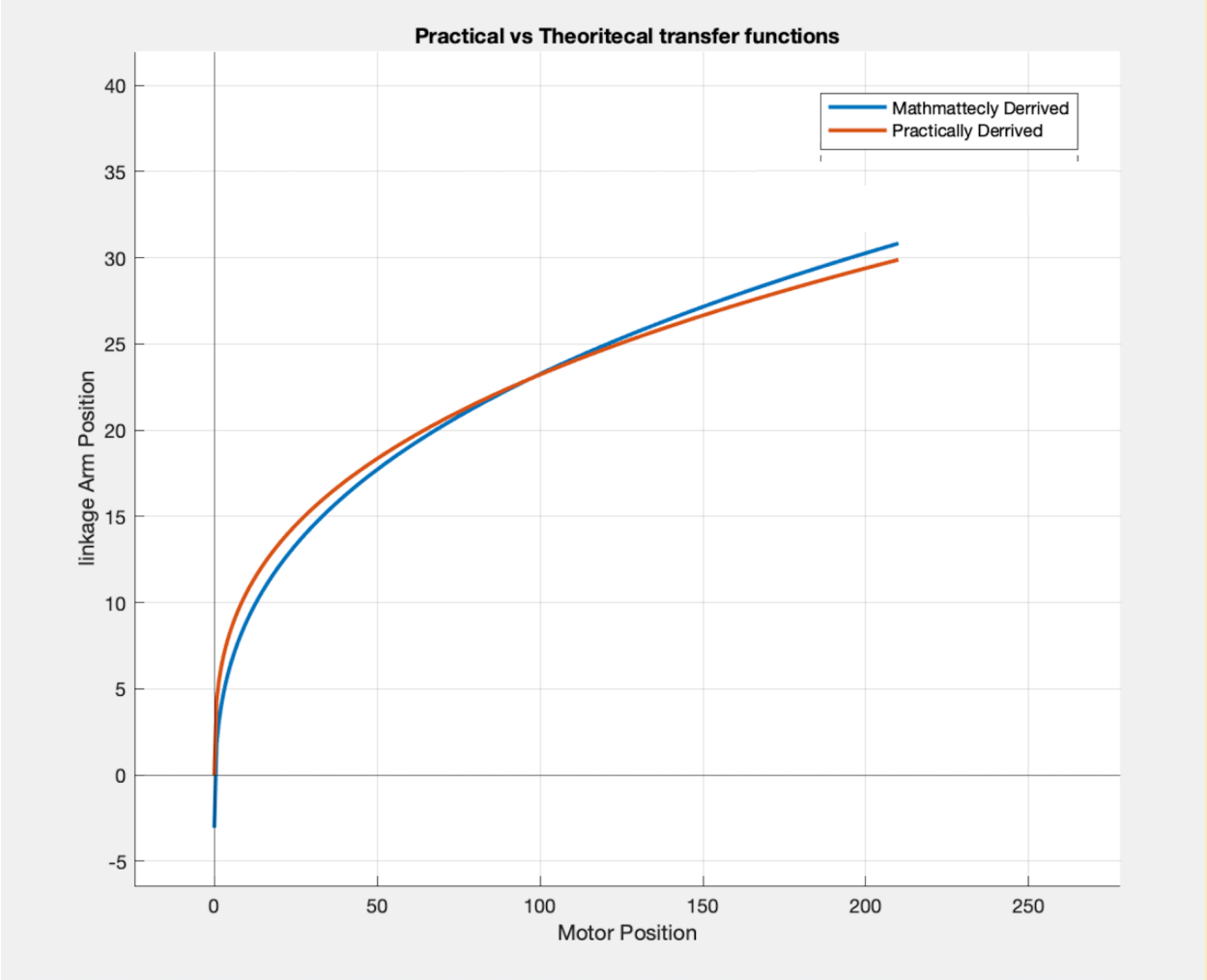

Figure 50: Comparing Transfer Functions

4.2 Capstan

4.2.1 Small Drum

After printing the first iteration of the small drum, we realize the angle of the groves wrapping the drum were incorrect. At the time of this print, there were also groves on the large drum and after assembly with the cord, it was apparent that the groves did not align to allow for smooth travel of the cord between the two surfaces. From this we learned the coil angle of the grooves needed to match rather than the pitch.

For the next iteration of the small drum, we decreased the angle of the groves and increased the number of groves to allow for more wraps around the drum. The increased contact area between the cord and the drum decreased the likelihood of slipping and ensured tension remained in the system. It did, however, also increase the hoop stress on the small drum, so we elected to print the small drum from resin for the next iteration.

The first resin print of the small drum was relatively successful but had some flaws including print quality. Although the resin proved to be strong, the orientation at which we printed it caused supports to connect to the grooved surface. After removing the supports the surface had residual bumps within the groves which affected the drums ability to roll smoothly along the large drum. The bumps also encouraged the cord to walk and sometimes overlap on itself. To remedy this, for the next prints we chose a print orientation where the supports did not make contact with the grooved surface and produced successful results.

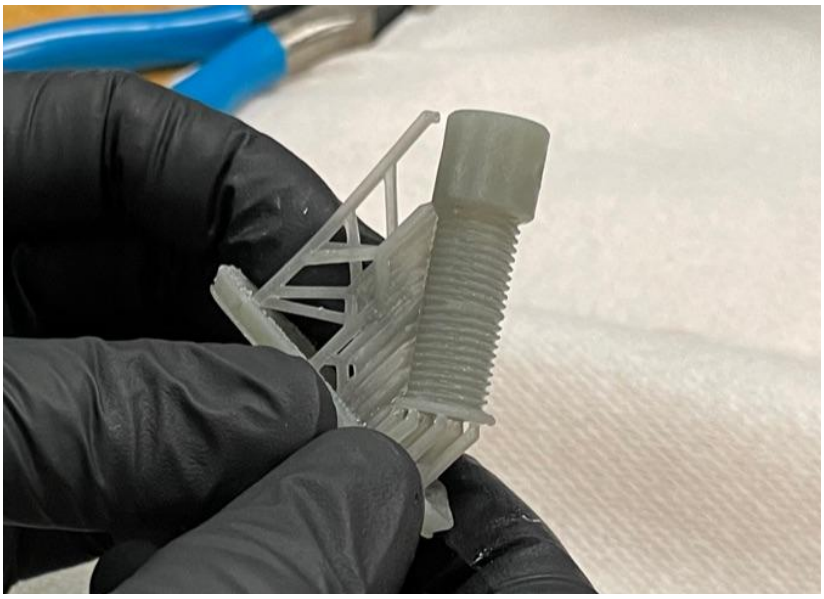

Figure 51: Supports Interacting with Grooves on Resin Printed Small Drum

An aluminum version of the small drum was later produced in order to solve the strength issues seen with the resin printed small drum. This aluminum small drum performed well in that respect, not bending at all when the dyneema was fully tensioned and the suspension moved. However, it was unable to be used in testing as it did not have high enough friction to the dyneema leading to significant slippage even at forces well below those required to dampen the suspension.

To increase the frictional problems seen with the aluminum drum, we combined the strength benefits of the aluminum and the friction of the resin. This drum was a hybrid drum consisting of an aluminum core and a resin sheath. The aluminum core provided the strength required to combat the tensional loads on the system from the dyneema. This drum was also doubly supported on both sides to reduce the load on the motor and the bending moment on the drum. We super glued the resin sheath onto the aluminum core to increase the friction as well as add the necessary groves. This drum exceeded strength requirements, but still experienced slip under the dynamic loads of testing.

4.2.2 Large Drum

Through the iteration of the large drum, we made many changes. First, we eliminated the groves designed into the large drum of the capstan. Removing the grooves and separating the

large drum into the main body and the crust made the manufacturing much easier and allowed for quick iteration of the thread profiles. Additionally, the large drum was modified to account for the updated tensioning system which included changing the torsion bar clamp to add the tensioning screw and moving the crust mounting hardware to one side to oppose the force of the tensioner.

4.2.3 Crust

The initial concept of the crust was sound, however, we decided to remove the grooves due to manufacturing requirements and research into other capstans that showed grooves were not necessary. To ensure stability of the cord without the grooves, we added the slots on the edges of the crust shown in Figure 52. We also moved the holes for the screws that fasten the crust to the large drum. Moving the fasteners closer to the hooked end of the crust countered the moment caused by the cord being tensioned on the opposite side. After increasing the number of wraps on the small drum, we also widened the crust which allowed the small drum to roll smoothly.

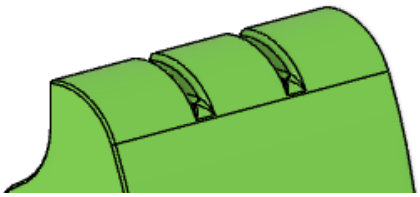

Figure 52: Cord Alignment Slots on Crust

4.2.4 Tensioner System

Based on the initial theory of tensioning including epoxy strand end anchors and sliding cylindrical drum tensioners, we chose to apply the guitar tuning peg tensioner to the first few prototypes of the capstan. Because of simplicity and availability, we were able to base the printed prototypes off of the tuning peg fairly easily. When initially doing our proof of concept tests for the capstan, the tuning peg was functional for the purpose of tensioning the Dyneema around the drums.

Because of this success we decided to simplify the design of the tensioner and machine a shoulder bolt to function as a tensioner. The concept of twisting the peg/ bolt was consistent through both prototypes, however after testing the shoulder bolt tensioner we realized the crucial component in the tuning peg is the internal worm gear to prevalent the system for being back driven and releasing tension. During the test, even with a set screw engaging with the shoulder bolt tensioner, the rotational force of the cord around the bolt would unscrew it and release tension.

Based on these results we changed direction and designed a tensioner more similar to our initial research. This tensioner system consists of the extended clamp, the tensioning plate and the tensioning screw. Nomenclature can be seen in Figure 53 below. After initial assembly, this tensioning system was clearly more effective than the shoulder bolt tensioner as it did not settle

nearly as much and remained in good tension for over 48 hours. When rolling the small drum, the cord remains taught and the tensioner seems to function as intended.

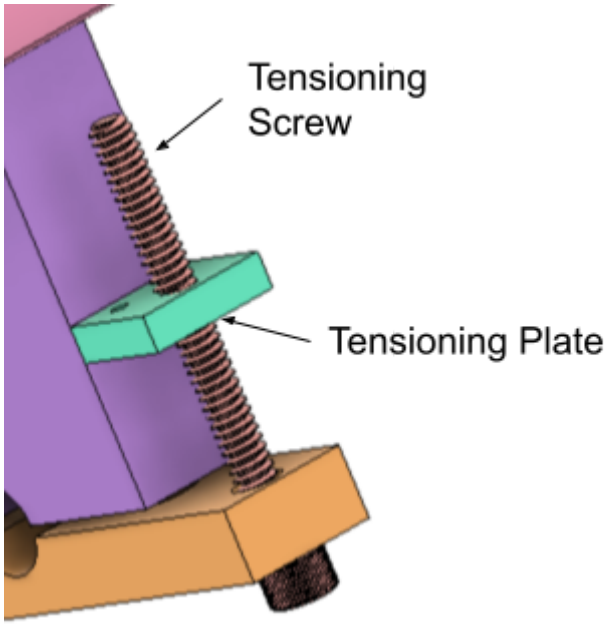

Figure 53: Linear Tensioner Nomenclature

4.3 Torsion Rod/ Clamps

4.3.1 Knurling Operation

After performing the knurling operation we had a few key takeaways. Firstly, because knurling is a forming operation, the tool enacts a large force on the stock. A spot drill on the end of the stock opposite the chuck was created to use the tail stock and ensure the rod did not bend during knurling. We also learned that the circumference of the knurling tool is an important dimension when deciding which tool to use. If the rod has a circumference divisible by the distance between the teeth on the knurling tool, the imprints will overlap as the rod rotates rather than becoming offset from each other. This difference can be seen in Figures 54 and 55.

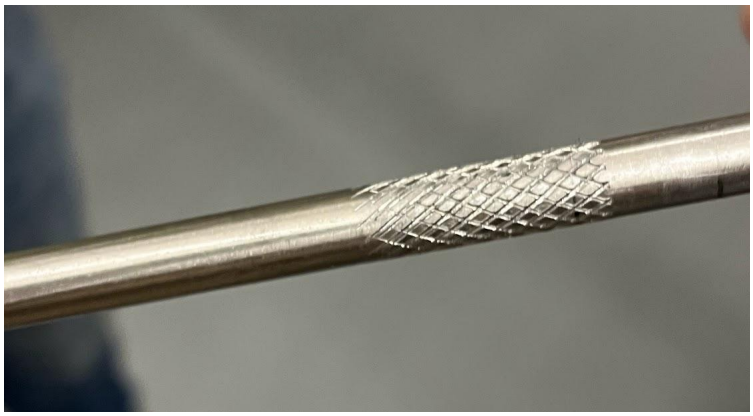

Figure 54: Knurling with Repeating Imprints

Figure 55: Knurling with Offset Imprints

4.3.2 Testing

The steel rod slip test produced results that lead us to the decision of continuing with our previously designed clamp. When testing the clamp on the smooth surface of the steel rod, we induced slip in the clamp by enacting 39 ft.lbs of torque on the torsion rod. When testing the clamp on the knurled surface, we did not induce slip before the steel rod bent. The maximum force applied to the rod whilst clamped on the knurled section was 62 ft.lbs. From these results we deduced knurling the surface of a rod leads to more success when clamping.

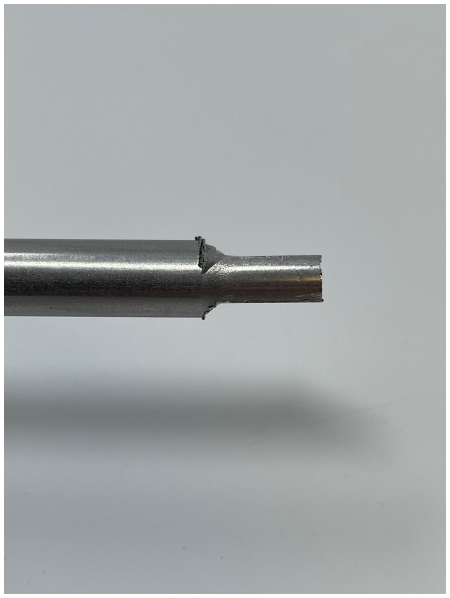

Figure 56: Bending of Steel Rod During Slip Test

4.4 Motor

4.4.1 Active Damping

Using the test fixture, we tested various control algorithms.

One-way damping: This system would not damp for compression of the system and would begin damping on the return. This yielded very good bump compliance with good damping on the return to prevent overshoot. One concern with this control algorithm is that it would not handle small road vibrations very well due to not being able to identify what state the suspension is in purely with encoder data.

Position control: This system would damp more as you get further from the center, This created a torque that almost negated the spring force at all positions due to both forces being linearly related to the change in angle.

Velocity control: This yielded the best results and was a successful start for the control system. Velocity control damps high frequencies well while allowing lower frequencies through undamped.

4.4.2 Regenerative Damping

Using the drill, we found that spinning the motor produced a small voltage gain in the battery. This proved that this motor is capable of regenerating voltages at speeds within the range of our system.

4.5 Assembly/Testing

4.5.1 Skeleton CAD Modeling Strategy

Skeleton modeling led to a robust assembly that could have core dimensions changed without breaking the structure or motion of the CAD model. Skeleton modeling is an incredibly robust way to organize CAD assemblies where there are many rigid subassemblies and iteration will be required.

Some of the difficulties of skeleton files arise where large groups of people have to edit the same assemblies. Due to the nature of all critical dimensions needing to be placed on the skeleton file in order to maintain its robustness, and not having the ability for work to sync without saving and sending to other editors, the use of skeleton files make it difficult for more than one person to be working on the same assembly at the same time. Skeleton files benefit from good communication among team members when pushing and pulling of files to the collaboration environment of choice (in our case Grabcad).

4.5.2 Assembly

Through iteration of this system, we learned that designing an order of operations within the assembly is important for the ease of putting the system together, as well as making changes to the prototype. Our system required a high level of disassembly in order to change, modify, or fix parts of the fixture. This was cumbersome and time-consuming. A better assembly process would have allowed us to iterate faster and make more changes to the system.

4.5.3 System Response testing

The data in Figures 57 and 58 shows the results from the system response testing from a 100N load being released from the linkage arm. The graph shows that the system experiences oscillations with damping scalar factors below 25. This shows us that with this test, a scaling factor of roughly 30 would result in a critically damped response. The discrepancies of the ending position can be explained by slipping of the cable on the small drum.

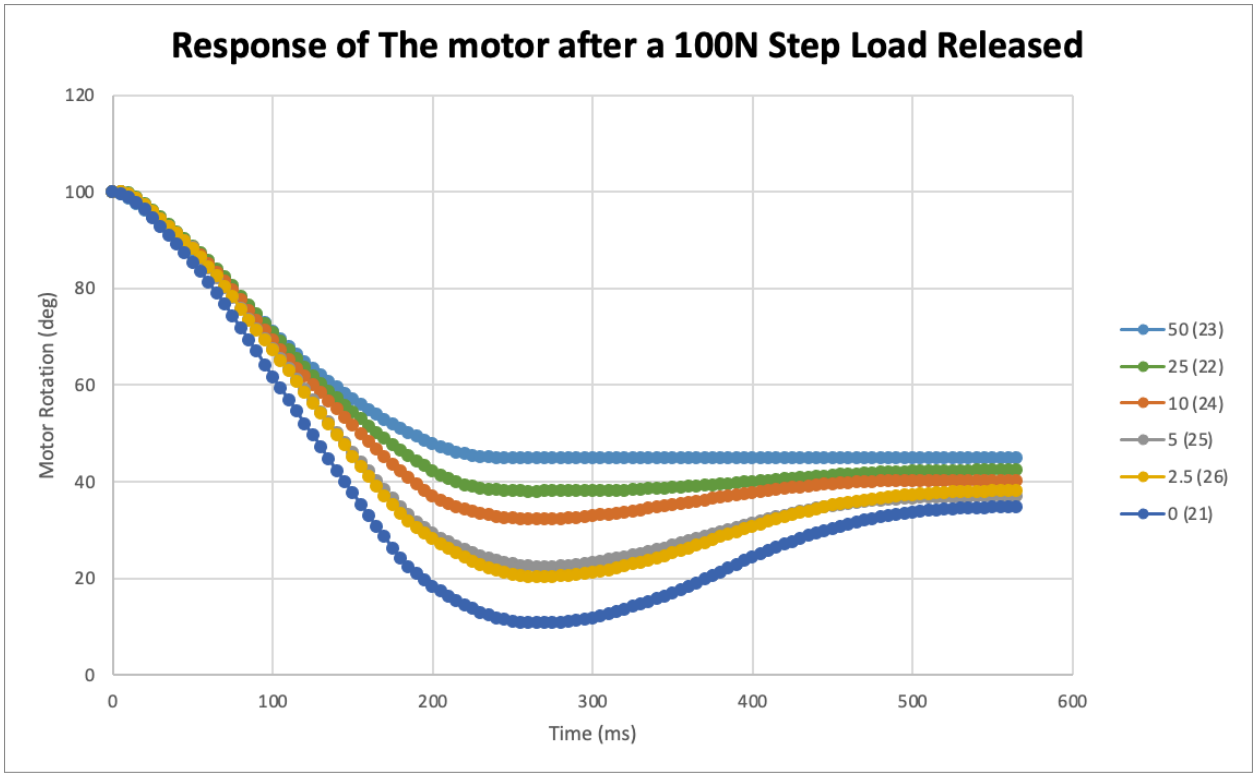

Figure 57: Response of the Motor after Release of 100N Load

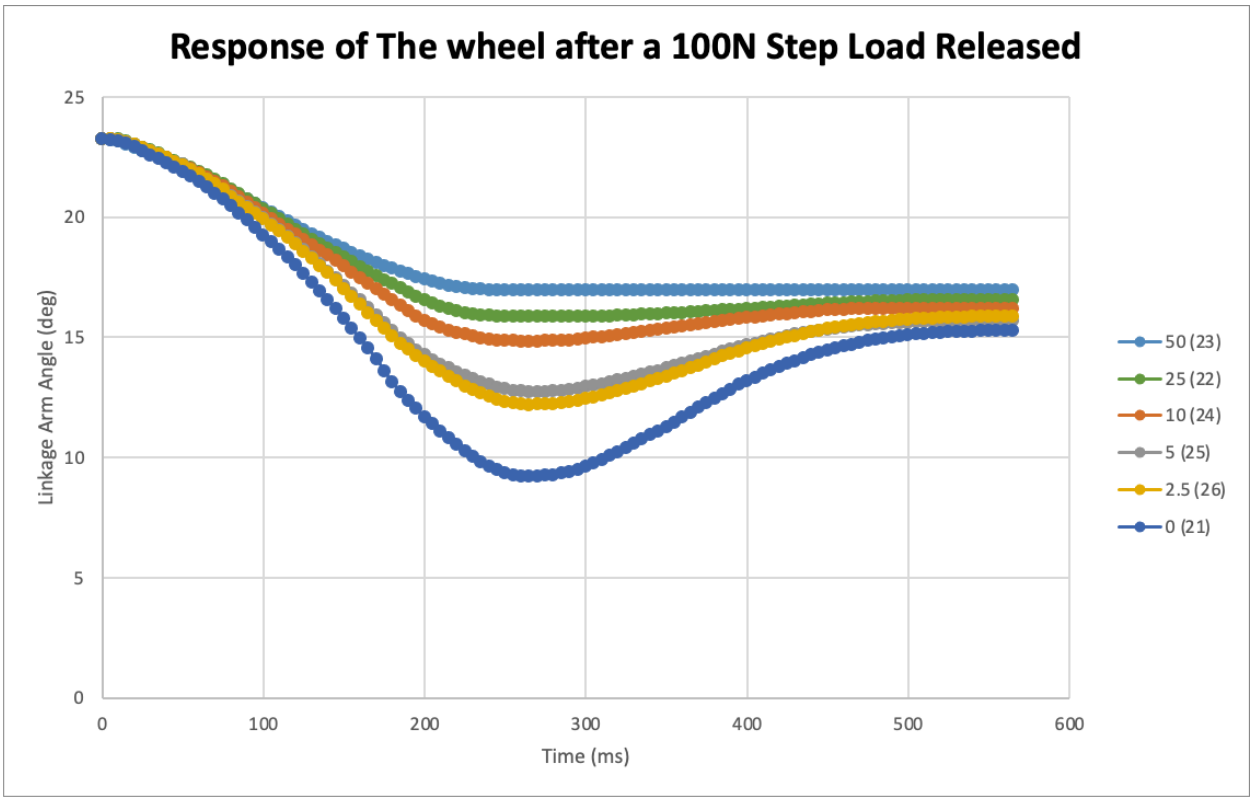

Figure 58: Response of the Linkage Arm after Release of a 100N Load

Through this testing, we found multiple components of the design that did not withstand the high loads of testing. One component was the ¼” live shaft that interfaced with the slot. This shaft was double supported with the linkage arms and retained in ball bearings, but the shaft bent under the loads of testing. We calculated that the maximum load on this bar was 1400 lbs which is far too high for a ¼” steel shaft. To improve this problem, we would either introduce linear slides instead of a live shaft, or design a much larger shaft to withstand the loads. We also saw slipping of the Dyneema cable on the small drum. This problem is discussed in section 6.

4.5.4 Motor Power Regeneration Testing

Test 1:

This test resulted in a peak voltage of 2 volts and shows that an oscillation of the system induces a current in the motor which can be collected with a battery.

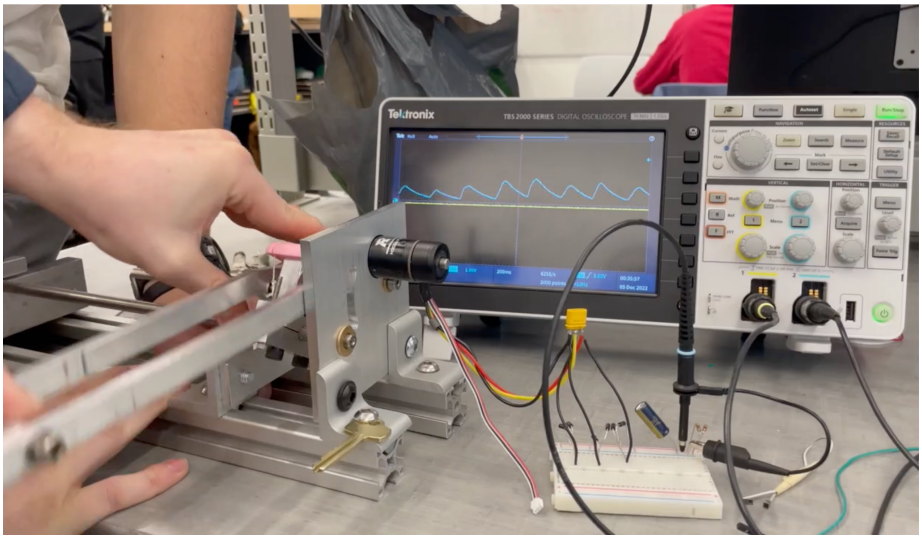

Figure 59: Motor Power Regeneration Testing

Test 2:

The data displayed in Figure 60 shows that the voltage increase per minute increases quadratically with the speed of the motor. This data can be used to predict the voltage increase of different inputs of the system.

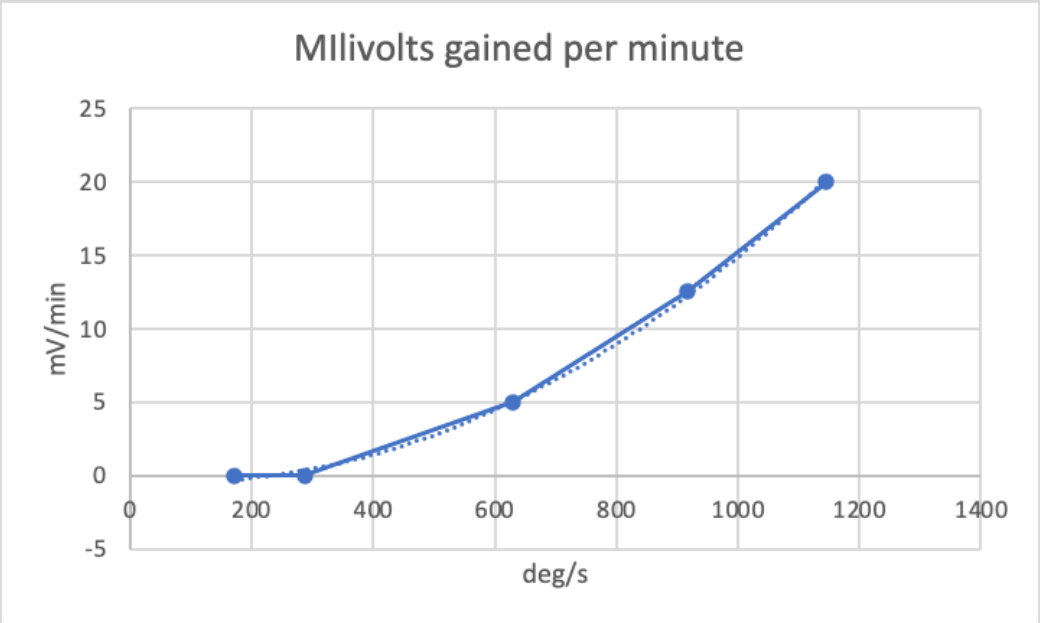

Figure 60: Voltage Increase as a Result of Test 2

5 Conclusion

- Our Slider linkage was functional but caused problems with binding and could be replaced with a linkage less likely to fail
- The linear tensioner concept was successful and held tension, but slipping still occurred in the capstan assembly due to slight hop in the small drum. Our knot for the cord on the capstan could also be improved upon to prevent slip
- The additional support plate and standoffs were necessary for proper alignment of the entire assembly and improved function substantially
- Our live shaft was not strong enough to handle the large loads in the system and should be replaced with something stronger in the future
- Our setup is able to charge a battery from movement of the suspension
- The overall assembly was functional as a suspension system and we were able to successfully control the damping coefficient of the system for many use cases

6 Future work

Throughout our testing there was a constant issue of the Dyneema slipping on the small drum. The major factors that contribute to this slippage are the number of wraps on the drum, the tension on the Dyneema, and the friction coefficient between the Dyneema and the drum. Increasing any of these factors could lead to the mitigation of this issue but some more innovative solutions could also be used.

In order to increase the friction factor between cable and the small drum you can change the surface finish of the material or change the material used entirely. The second of these two

options was utilized by switching from an aluminum small drum to a resin printed hybrid small drum, this was partially effective but did not entirely eliminate the issue. The use of a steel braided cable on aluminum could cause the steel to slightly bite into the drum increasing friction. Sandblasting the aluminum small drum could also have a positive impact on the friction coefficient leading to less slippage.

One observation made during testing was that the tension on the cable was not uniform. The precise reasoning for this is unknown but one possible source is small amounts of hop in the small drum. A way to mitigate the effects of this and therefore prevent slippage is attaching a spring to the tensioning system that provides a semi constant load to the cable regardless of a few millimeters of change in the loop length of the cable. This tensioning spring could be implemented between the bolt head and the tensioner as pictured below.

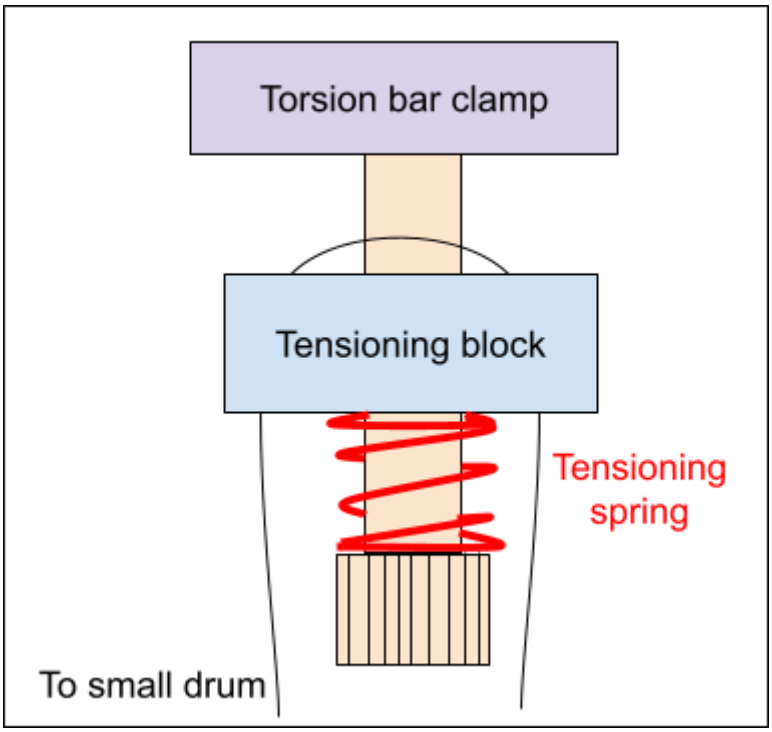

Figure 61: Linear Tensioner with Spring

Another possible solution to the Dyneema slipping on the small drum is terminating the wraps on the drum itself. To execute this you would have two different cables that would be tensioned on either side of the large drum as pictured below.

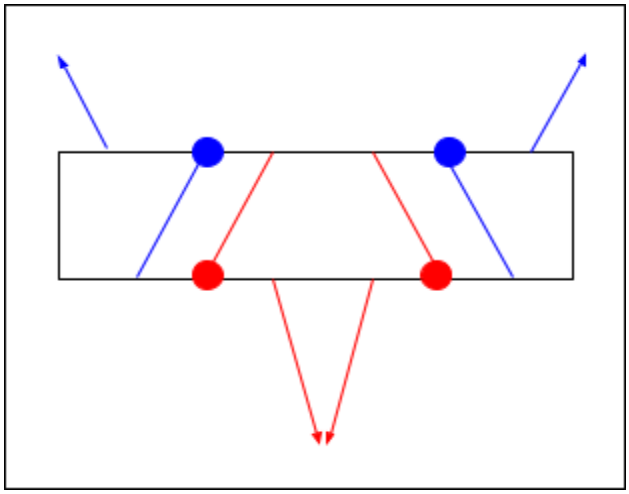

Figure 62: Small Drum with Cable Termination on Drum

Each cable would start at the drum terminated on or inside the drum, wrap around the small drum to the tensioner and back to the small drum where it would wrap back around and terminate. Since the small drum only needs to spin 300 degrees and the system no longer relies on friction only one wrap would be required meaning that the large and small drums could be more narrow, decreasing the overall weight of the system. This termination could take the form of a hole in the drum where the cable could be passed through, a knot could be tied in it which would then be epoxied to prevent it from slipping or coming undone.

We also experienced ~7 degrees of backlash from the motor shaft to the small drum. This backlash was caused by the set screw passing through the motor shaft tolerance to the hole in the motor shaft. One possible solution to this problem is machining the D into the small drum that the motor shaft that exists on the shaft. Another solution is using a set screw pin instead of a fully threaded set screw, a set screw could be used with a smooth shaft that is a much closer fit to the hole in the motor shaft. A final possible solution would be pressing a new shaft into the brushless motor that has an interference fit small drum already attached to it, this would also prevent any hop in the small drum.

More testing could also better inform future design changes and decrease slip between the cable and small drum. One useful test would be a longer term energy generation test with realistic road conditions. This test could be completed in many ways with different setups but two of the simplest are the use of a CNC mill, and a cam on a motor. The CNC path would require very little setup, the test fixture would be secured in the vice and a dowel pin placed in a collet in the spindle. The CNC machine would then be commanded to repeatedly depress the suspension by driving the dowel pin into it. The following code could be used:

```
G21 (sets units to mm)
G1 Z-25.4 F30000 (goes down 25.4 mm to -25.4 mm at 30000 mm/min)
G1 Z 0 F30000 (goes up 25.4 mm to 0 mm at 30000 mm/min)
```

```
G04 P400 (pause for 400ms)
G1 Z-25.4 F30000 (goes down 25.4 mm to -25.4 mm at 30000 mm/min)
G1 Z 0 F30000 (goes up 25.4 mm to 0 mm at 30000 mm/min)
G04 P400 (pause for 400ms)
```

Figure 63 G Code for CNC Energy Generation Test

This code could be used on the Haas Super Mini Mill and simulates driving over a one inch bump at 1.185 mph twice, repeating the last 3 lines an arbitrary number of times would simulate more bumps. Another way to do this testing less technically is to make a one inch offset cam, attach it to a motor, and have it spin repeatedly depressing the suspension, the apparatus would look like Figure 64 below.

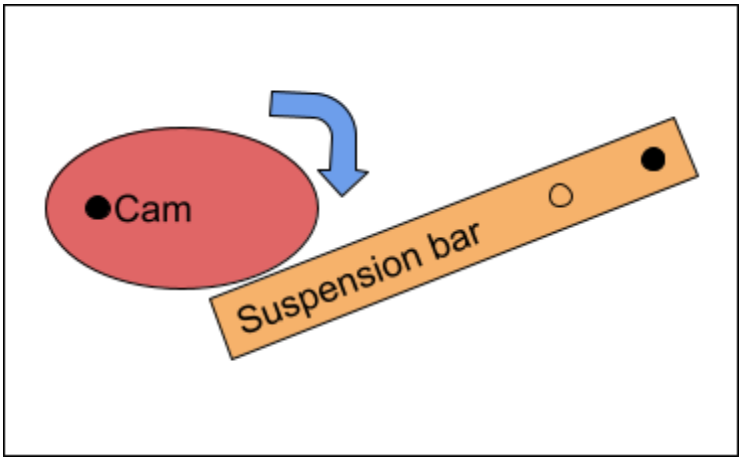

Figure 64:Cam Based Suspension Test Setup

There are also relevant tests for different ways of controlling the damping. This includes controlling damping based on position, velocity and acceleration. Damping can also be controlled based on the direction which would produce different damping on the compression and return of the system. Implementing and testing some of these different control algorithms may result in an algorithm that is best for this particular use case. We foresee different damping profiles for different riders, terrains, and conditions.

Appendix:

2.5 MATLAB Script for Identifying Ideal Torsion Bar Diameter and Effective Length

```
clear; clc;

G = 41;         %Shear Mod Grade V Ti (MPa)
La = 1.75;      %Twist arm length (in)
F = 81.75;      %Applied force (kg)
phi = 31;       %Torsion angle (deg)
d = 8:.01:10;   %Rod Diameter (mm), plotting ideal range between 8-10mm
```

```
G = G*10^9; % MPa to Pa
La = La * 25.4 / 1000; %Twist arm length (in to m)
F = F * 9.82; % kg-F to N
phi = deg2rad(phi); %Torsion angle
d = d / 1000;

Torque = F*La;

L = (phi*G*pi*power(d/2,4))/(2*Torque);
Stress = Torque*(d/2)./((pi/2)*power(d/2,4)*10^6); %MPa

figure(1); %Twistrod Length vs. Diameter
L = (phi*G*pi*power(d/2,4))/(2*Torque);
plot(d*1000,L)
grid on
title('Diameter vs Length & Stress')
xlabel('(mm)')
ylabel('(m)')

yyaxis right
plot(d*1000, Stress)
ylabel('(MPa)')
```

3.3 Clamp Torque Capacity Euations

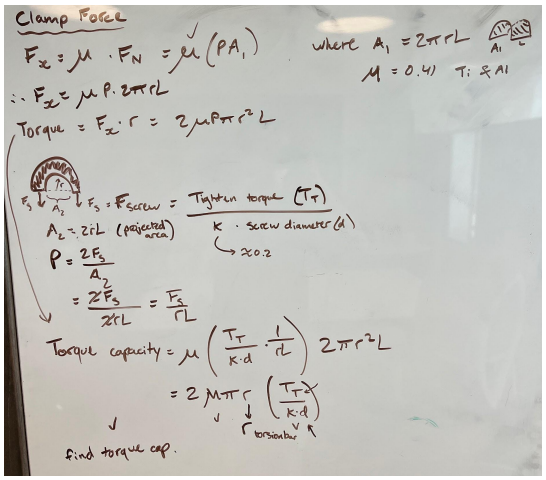

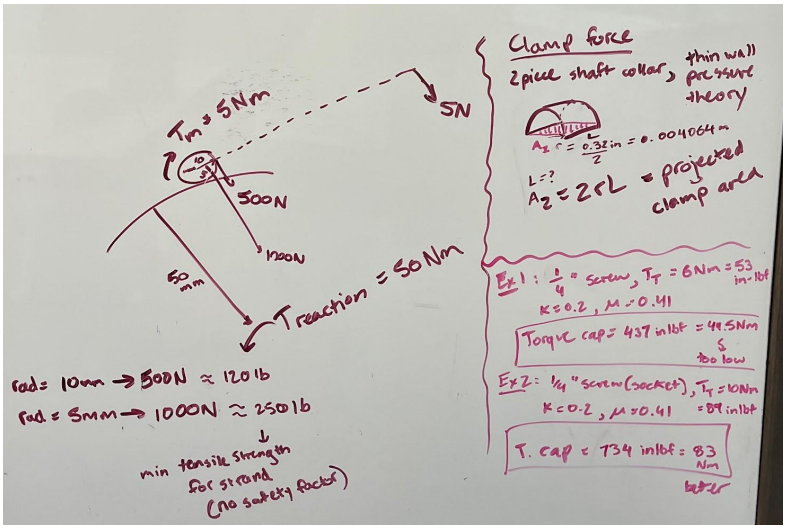

4.1.3 Slider Linkage Prototype Data

Linear Travel (cm)	Force (kg)			
Trial	Low Stiffness, Trial 1	Low Stiffness, Trial 2	High Stiffness, Trial 1	High Stiffness, Trial 2
1	0.07	0.09	0.16	0.19
2	0.11	0.14	0.27	0.31
3	0.18	0.23	0.42	0.49
4	0.27	0.31	0.64	0.73
5	0.33	0.44	0.87	0.95
6	0.44	0.59	1.28	1.39

4.1.4 MATLAB Script to Create Discrete Function Relating Motor Angular Position to Effector Arm Angular Position

V1 Transfer Function (300 degrees of motor travel)

```
% Transfer Function Relating Read Motor Angular Position to Change in Effector Arm Angle
clear; clc;
alpha = 0; % Motor Angular Position (deg)
b = 2.08714; % inches, base distance pivot axis to torsion rod axis
l = 1.63178; % inches, linkage "length" pivot axis to slider axis
phi_resting = 51.38;
theta_resting = 36.62;
i = 1; % Index
syms gamma

% Create discrete data relating alpha to phi
while alpha < 300 % While motor (alpha) is within expected range (0-300 deg of rotation
during suspension travel), calculate phi
    psi=  phi_resting - alpha*(30/300); % Phi = change in effector arm angle
    eq1 = sqrt(l^2 + b^2 - 2*l*b*cosd(gamma))*sind(psi) == l*sind(gamma);

    % Log each iteration of alpha and theta in equal size arrays
    motor_alpha(i) = alpha;
    theta(i) = double(theta_resting - vpasolve(eq1, gamma));

    % Index up
    i = 1 + i; % Index up one iteration
    alpha = alpha + 1; % Index up 1 degree per iteration
end
figure(1)
plot(motor_alpha,theta)
xlabel('Motor position (deg)')
ylabel('Effector arm angular travel (deg)')
```

4.1.4 V2 Transfer Function (210 degrees of motor travel)

```
% Transfer Function Relating Read Motor Angular Position to Change in Effector Arm Angle
% New TF using 210 degrees of motor rotation due to some backlash noted in
% system
clear; clc;
alpha = 0.001; % Motor Angular Position (deg)
b = 2.08714; % inches, base distance pivot axis to torsion rod axis
l = 1.63178; % inches, linkage "length" pivot axis to slider axis
phi_resting = 51.38;
theta_resting = 36.62;
```

```
i = 1; % Index
syms gamma

% Create discrete data relating alpha to phi
while alpha < 210 % NEW MAX ANGLE While motor (alpha) is within expected range
(0-210 deg of rotation during suspension travel), calculate phi
    psi =  phi_resting - alpha*(30/210); % Phi = change in effector arm angle, NEW ANGLE
    eq1 = sqrt(l^2 + b^2 - 2*l*b*cosd(gamma))*sind(psi) == l*sind(gamma);

    % Log each iteration of alpha and theta in equal size arrays
    motor_alpha(i) = alpha;
    theta(i) = double(theta_resting - vpasolve(eq1, gamma));

    % Index up
    i = 1 + i; % Index up one iteration
    alpha = alpha + 1; % Index up 1 degree per iteration
end
figure(1)
plot(motor_alpha,theta)
xlabel('Motor position (deg)')
ylabel('Effector arm angular travel (deg)')
```

Bibliography:

Liu, Y., Feng, X., Li, Y. *et al.* Research on boundary slip of hydrostatic lead screw under different driving modes. *Sci Rep* 11, 22307 (2021). https://doi.org/10.1038/s41598-021-01524-8

"About the G4 Range." *BajaBoard*, https://www.bajaboard.com.au/pages/about-g4.

Perkins, Chris. "How Formula 1 Suspension Works." *Road & Track*, Road & Track, 1 May 2021, https://www.roadandtrack.com/car-culture/a35645925/how-formula-1-suspension-works/.

Kahraman, A., Li, S. (2013). Friction in Gears. In: Wang, Q.J., Chung, YW. (eds) Encyclopedia of Tribology. Springer, Boston, MA. https://doi.org/10.1007/978-0-387-92897-5_675

Simmons, Colin H., et al. "CAMS and Gears." *Manual of Engineering Drawing*, 2020, pp. 421–444., https://doi.org/10.1016/b978-0-12-818482-0.00031-1.

"Introduction: The Main Types of Braided Structure Using Maypole Braiding Technology." *Braiding Technology for Textiles*, 2015, pp. 1–25., https://doi.org/10.1533/9780857099211.1.

T. Ishida and A. Takanishi, "A Robot Actuator Development With High Backdrivability," 2006 IEEE Conference on Robotics, Automation and Mechatronics, 2006, pp. 1-6, doi: 10.1109/RAMECH.2006.252631.

A. Mazumdar et al., "Synthetic Fiber Capstan Drives for Highly Efficient, Torque Controlled, Robotic Applications," in IEEE Robotics and Automation Letters, vol. 2, no. 2, pp. 554-561, April 2017, doi: 10.1109/LRA.2016.2646259.

"Introduction: The Main Types of Braided Structure Using Maypole Braiding Technology." *Braiding Technology for Textiles*, 2015, pp. 1–25., https://doi.org/10.1533/9780857099211.1.

Collins, Sam. "J Dampers in Formula One." *Racecar Engineering*, 24 Apr. 2018, https://www.racecar-engineering.com/articles/f1/understanding-the-j-damper/.

Kay, Mark. "Tech Draft: Farewell to the Jounce Damper." GRAND PRIX 247, 18 Jan. 2022, https://www.grandprix247.com/2022/01/18/tech-draft-2022-2-farewell-to-the-jounce-damper/.